Geophysical Journal International

Geophys. J. Int. (2011) **185,** 1288–1304 doi: 10.1111/j.1365-246X.2011.04995.x

Asymmetric distribution of aftershocks on large faults in California

Ilya Zaliapin[1] and Yehuda Ben-Zion[2]

[1]*Department of Mathematics and Statistics, University of Nevada, Reno, NV* 89557*, USA. E-mail: zal@unr.edu*
[2]*Department of Earth Sciences, University of Southern California, Los Angeles, CA* 90089-0740*, USA*

Accepted 2011 February 22. Received 2011 February 22; in original form 2010 January 25

SUMMARY

We examine the relations between spatial symmetry properties of earthquake patterns along faults in California (CA) and local velocity structure images to test the hypothesis that ruptures on bimaterial faults have statistically preferred propagation directions. The analysis employs seismic catalogues for 25 fault zones in CA. We distinguish between clustered and homogeneous parts of each catalogue, using a recently introduced earthquake cluster analysis, and examine asymmetry of offspring with respect to parent events within the clustered portion of each catalogue. The results indicate strong asymmetric patterns along large faults with prominent bimaterial interfaces (e.g. sections of the San Andreas Fault), with enhanced activities in the directions predicted for the local velocity contrasts, and absence of significant asymmetry along most other faults. Assuming the observed asymmetric properties of seismicity reflect the properties of the parent earthquake ruptures, the discussed methodology and results can be used to develop refined estimates of seismic shaking hazard associated with individual fault zones.

Key words: Persistence, memory, correlations, clustering; Spatial analysis; Earthquake dynamics; Earthquake interaction, forecasting, and prediction; Statistical seismology.

1 INTRODUCTION AND MOTIVATION

Establishing whether there are genuine patterns of seismicity that may reflect local spatial or temporal properties of faults or the crust, beyond the well-known average regional patterns, remains an extremely challenging problem because of the inherent complexity of the earthquake process combined with the limited and noisy available data. Purely statistical studies tend to analyse seismicity associated with large spatial domains to increase the amount of data. However, this approach may suppress possible important aspects of seismicity that are specific to certain classes of faults. An ability to establish correlations between features of seismicity in specific subregions and independent geophysical observations can increase the information content of the available data and provide fundamental input for numerous studies ranging from theoretical investigations of earthquake physics to practical calculations of seismic hazard (e.g. Ben-Zion 2008). In this paper we analyse spatio-temporal properties of seismicity along individual fault zones in California (CA), and find that earthquakes on large faults, which separate different rock bodies (bimaterial faults) have special properties related to the local seismic velocity structure.

Theoretical studies indicate (e.g. Weertman 1980; Andrews & Ben-Zion 1997; Ben-Zion 2001; Shi & Ben-Zion 2006; Ampuero & Ben-Zion 2008; Brietzke *et al.* 2009) that ruptures on bimaterial faults have larger slip-velocity and slip in the direction of particle motion in the compliant solid (referred to as the preferred direction). The results stem from dynamic changes of normal stress (σ_n) near the tips of ruptures on bimaterial faults, which do not exist for faults separating similar elastic solids. For typical subshear ruptures the change of σ_n at the tip propagating in the preferred direction is tensile, while the change at the tip propagating in the opposite direction is compressive. The amplitudes of the dynamic changes of σ_n near the rupture tips increase with propagation distance along the bimaterial interface due to a continual transfer of energy to shorter wavelengths (e.g. Adams 1995; Ranjith & Rice 2001; Ben-Zion & Huang 2002). Therefore the dynamic bimaterial effects become progressively more important with increasing event size. The theoretical studies on this topic indicate (see discussion section) that bimaterial ruptures tend to be associated with larger moment release and larger generated motion in the preferred direction (Fig. 1). These results can have significant effects on the seismic shaking hazard in major metropolitan areas (e.g. Los Angeles, San Francisco and Istanbul) near large plate-bounding bimaterial faults (e.g. the San Andreas and North Anatolian Faults).

The asymmetric along-strike rupture behaviour on bimaterial faults is expected to produce two effects on the spatial distribution of aftershocks; one related to the rupture itself and concentrated at short distances from the arrested crack tips, while the other associated with the radiated waves and occurring over larger distances (but typically with small stress amplitude). Specifically, asymmetric ruptures (1) 'plow' further in the preferred direction and (2) can also generate enhanced ground motion at larger distances in the preferred direction. Process (1) is expected to produce more immediate aftershocks in the 'opposite' along-strike direction, since potential

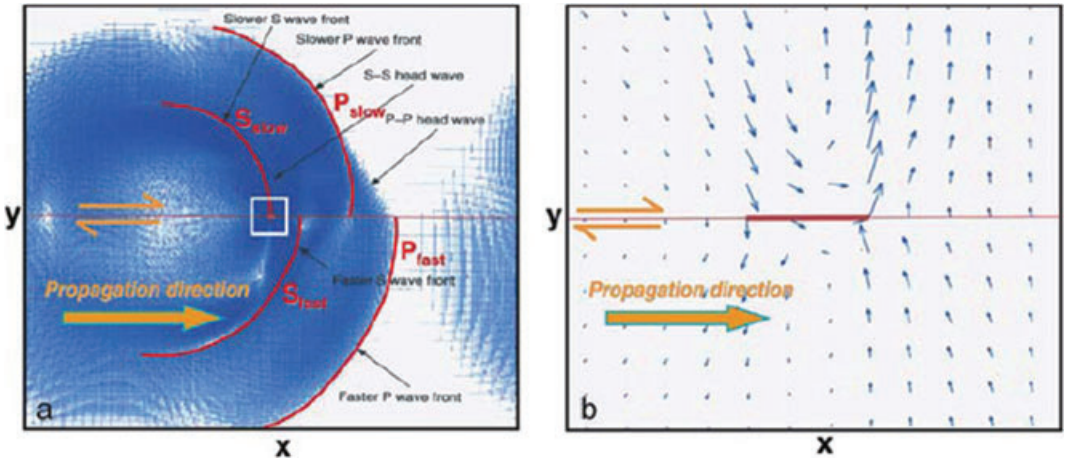

Figure 1. Particle velocities at a given time generated by a rupture pulse (small red bar in the white box on the left-hand side, shown in larger detail on the right-hand side) propagating to the right along a right-lateral strike-slip fault (thin red horizontal line) between different elastic solids. The top material has 20 per cent lower shear wave velocity than the bottom one. The asymmetric dynamic stress fields at the opposite rupture tips produce a statistical tendency of ruptures to propagate further to the right and include more potential sites of immediate aftershocks in that direction. This is expected to produce over very short space-time scales more aftershocks in the opposite along-strike direction. On larger space-time scales the rupture directivity is expected to produce more events in the far field of the propagation direction (after Ben-Zion 2001).

sites of immediate aftershocks in the propagation direction are more likely to fail as part of the parent events (Rubin & Gillard 2000). Process (2) is expected to produce more events in the far field of the propagation direction. This effect is familiar since large unilateral ruptures (like the 1992 Landers and 2002 Denali earthquakes) generate pronounced triggering in the propagation direction and associated clear large-scale aftershock asymmetry. Although the 'common seismological wisdom' is associated with large earthquakes and process (2), for small main shocks process (1) can be more dominant. This is because the near crack-tip stress fields can be significant (e.g. compared to a typical stress drop of ∼3 MPa) even for small events, but the wave-mediated stress changes in the far field are fairly weak for small earthquakes and become significant only for events with magnitude larger than ∼5.5. This estimate is based on peak ground velocities summarized by Atkinson & Boore (1997) and assuming that 1 cm s^{-1} produces ∼0.1 MPa. Statistical tests of the discussed effects require analysis of many earthquake sequences on a given fault, which necessitates using main shocks with low magnitudes. This is challenging but can be done by careful analyses of seismic catalogues and stacking of results.

In this paper we focus on behaviour of earthquakes on a set of large strike-slip faults with different degrees of velocity contrast. Repeating occurrence of ruptures with a statisitically preferred propagation direction on large strike-slip faults is expected to produce over multiple earthquake cycles asymmetric rock damage across the fault, with more shallow damage on the stiffer side (Ben-Zion & Shi 2005). Analyses of seismic fault zone waves and geological signals in the structures of the San Andreas, San Jacinto and North Anatolian faults revealed strongly asymmetric damaged fault zone layers as expected for bimaterial ruptures (Lewis *et al.* 2005, 2007; Dor *et al.* 2006a,b, 2008; Wechsler *et al.* 2009). However, these results are associated with indirect signatures of the earthquake behaviour on the examined fault structures. Rubin & Gillard (2000) and Schorlemmer & Ben-Zion (2008) presented evidence for asymmetric patterns of immediate aftershocks on the Northern San Andreas Fault (SAF), which has a clear velocity contrast. In addition, Rubin (2002) showed that the immediate aftershocks on the Calaveras Fault, which separates similar crustal blocks, are approximately symmetric in the different along-strike directions. Although these studies provide important high-resolution results, they are associated with a very small set of fault sections and should be substantiated by a more comprehensive analysis employing a larger data set. In this study we use a novel statistical approach to examine the along-strike symmetry properties of seismicity associated with 25 individual fault zones in CA.

We find that in zones with significant velocity contrast (> ∼5 per cent) more immediate spatially close offspring events tend to occur in the opposite along-strike direction, while later and more distant events tend to be enhanced in the preferred direction. In the zones with no-to-mild contrast the combined offspring distribution is statistically symmetric with respect to the parent events at all examined spatio-temporal scales. The observations demonstrate that there are clear differences in the spatio-temporal seismicity patterns along faults with and without significant velocity contrast. The results are consistent with the theoretical expectations that ruptures on bimaterial faults have asymmetric dynamic crack-tip stress fields and statistically preferred propagation directions related to the local velocity structure.

2 DATA

2.1 Fault zones and earthquakes catalogues

We analyse seismicity located within well-defined fault zones in CA, which makes the interpretation of our results on spatial symmetry properties particularly straightforward. Specifically, we focus on 25 seismic zones defined by Powers & Jordan (2010) and analyse the earthquake locations along the respective faults (Fig. 2). The employed catalogues are not dominated by large aftershock sequences (such catalogues are not used here), so the results should reflect persistent statistical behaviour of seismicity in the various examined zones. In southern CA, the catalogues of Powers & Jordan (2010) are based on two relocated catalogues, Hauksson & Shearer (2005) and Shearer *et al.* (2005), while in northern CA they are based on the catalogue of Ellsworth *et al.* (2000). Table 1 and Fig. 2 describe the essential features of the seismic catalogues used in this study. For additional details on the catalogues, see Powers (2009). We consider only a 1-D projection of the hypocentres on the fault

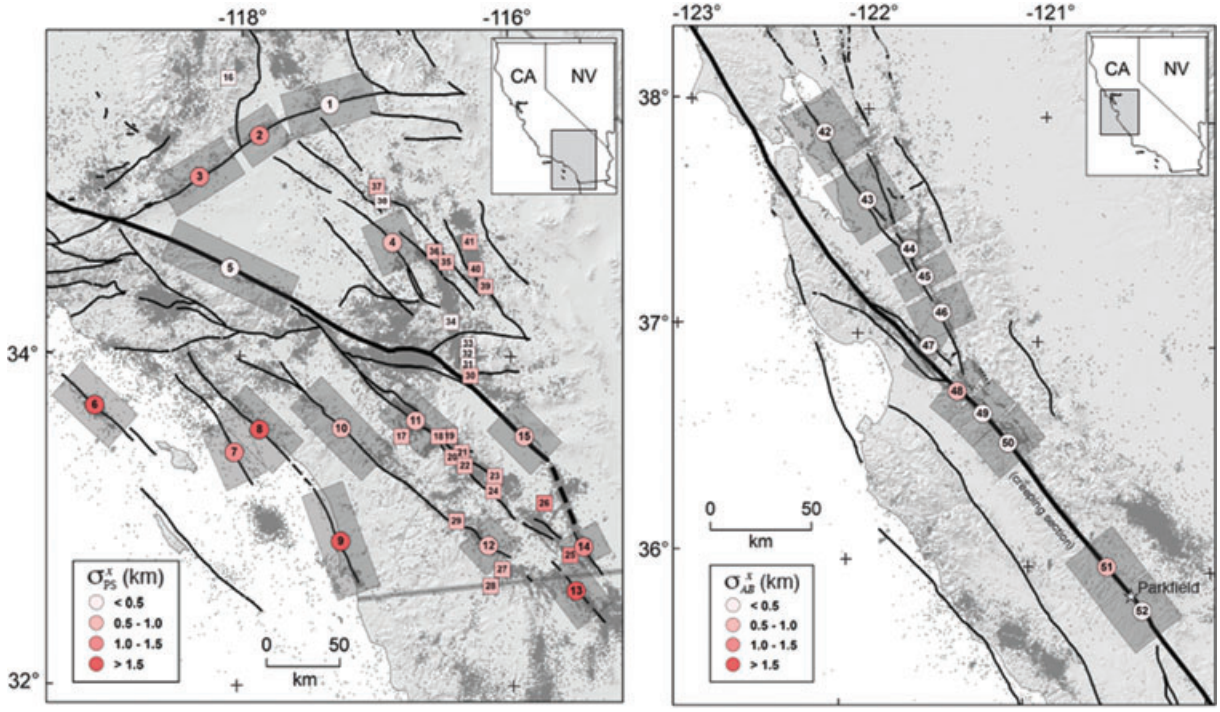

Figure 2. Location map of seismically active fault zones. The zone indices in circles indicate regions analysed in this study, while the zone indices in squares indicate aftershock-dominated zones that are not analysed here (after Powers & Jordan 2010).

Table 1. Fault zone description (strong contrast zones are shown in bold, see Table 2). Columns 5–8 show the numbers that correspond to $T_0 = 10^{-2}$, $R_0 = 3$ and minimal magnitude of 1.5.

Zone	1 Time span	2 Ave. depth (km)	3 Max m	4 No. events	5 No. MS[a]	6 Per cent MS[b]	7 C_5[c]	8 $<L_5>$[d]
1	1984.00–2002.98	9.21	4.09	1255	338	27	11	25.00
2	1984.03–2002.80	7.80	3.43	1174	327	28	28	12.64
3	1984.07–2002.95	5.25	4.18	1300	328	25	30	16.10
4	1984.38–2002.98	7.66	4.36	291	116	40	5	23.40
5	**1984.01– 2002.93**	**9.51**	**4.40**	**1227**	**371**	**30**	**10**	**14.10**
7	1984.08–2002.93	8.40	4.83	489	365	75	3	14.00
8	1984.08–2002.97	10.16	4.83	452	304	67	3	23.33
9	1984.07–2002.94	9.82	3.87	346	205	59	4	21.25
10	1984.06–2002.98	9.68	3.25	989	301	30	7	9.29
11	1984.00–2003.00	13.81	4.15	7802	2119	27	100	14.89
12	1984.05–2002.88	9.92	3.98	754	251	33	6	12.00
13	1984.07–2002.98	10.38	4.03	1640	743	45	32	11.25
14	1984.01–2003.00	12.67	3.81	1626	734	45	22	10.00
15	**1984.03–2002.78**	**6.71**	**3.27**	**606**	**190**	**31**	**15**	**11.87**
42	**1984.39–2000.87**	**9.16**	**4.12**	**530**	**222**	**42**	**8**	**11.63**
43	1984.34–2000.86	7.91	4.40	2151	464	22	28	22.18
44	1984.33–2000.86	6.08	5.00	3863	446	12	63	27.70
45	1984.33–2000.85	4.17	3.66	772	82	11	13	10.62
46	1984.33–2000.88	4.69	5.10	3021	335	11	50	22.76
47	1984.33–2000.88	5.73	4.16	2109	282	13	31	15.52
48	**1984.33–2000.91**	**5.17**	**5.35**	**3762**	**462**	**12**	**78**	**20.69**
49	1984.33–2000.90	6.00	4.70	4601	686	15	79	26.80
50	1984.33–2000.91	6.33	5.14	8806	1102	13	125	32.61
51	**1984.01–2002.50**	**4.87**	**5.03**	**3995**	**769**	**19**	**45**	**17.47**
52	1984.01–2002.49	8.03	3.99	565	156	28	3	7.67

[a,b]MS = mainshock (the first event of maximal magnitude in a cluster); the number of mainshocks equals the number of clusters.
[c]C_5 = number of clusters with more than five events.
[d]$<L_5>$ = average no. of events in clusters with more than five events.

line associated with each zone. This intentional reduction of spatial-information helps us to focus on the along-strike properties of the catalogues. In our analysis each earthquake i is characterized by its 1-D spatial projection x_i on the fault line, time t_i and magnitude m_i.

The catalogues used in the study are based on a mixture of methods for determining the earthquake locations. The locations of smaller earthquakes (or at least their relative locations) are determined in most cases by waveform cross correlations and thus better approximate the event centroids. The locations of larger earthquakes are more likely constrained by arrival-time picks, meaning that the relative locations better approximate the hypocentre than the centroid (Peter Shearer, personal communication, 2010). The mixture of hypocentre and centroid locations might affect the results of statistical analyses relying on locations. To minimize these effects, we analyse separately in Section 4.2 earthquakes with magnitudes below and above 3. Moreover, we perform a separate analysis of offsprings at large distances from the parents, the results of which are independent of the location type. The combined set of analyses performed in this study allows us to obtain results that are robust with respect to the mixture of event's location type.

The examined catalogues are associated with strike-slip faults. We adopt the following notation based on the theoretical expectations associated with bimaterial ruptures (e.g. Weertman 1980; Ben-Zion 2001). If the examined catalogue is associated with a right-lateral fault and the top material, when viewed in a plot like Fig. 1, has lower seismic velocity, the theoretically preferred propagation direction is to the right. If the catalogue is associated with a left-lateral fault (which is relevant here only for the Garlock fault in zones 1–3), or if the top material (when viewed in a plot like Fig. 1) has higher seismic velocity, the preferred propagation direction is to the left. As mentioned, the expected asymmetry on a short space–time scale is in the opposite direction to the preferred propagation direction. These notations are used to construct the entries on 'Preferred direction' and 'Expected asymmetry' in Table 2. On the other hand, when analysing the observed seismic catalogues we wish to have a simple geographical definition for positive and negative asymmetries of seismicity. In this context we adopt the following terminology. An excess of seismicity in the northwest (NW) or northeast (NE) directions is referred to as positive asymmetry, while access of seismicity in southwest (SW) and southeast (SE) correspond to negative asymmetry. These notations are used to construct Figs 8 and 9.

2.2 Fault velocity contrasts

Summarizing information on the velocity contrasts across the examined faults is not straightforward, because of non-uniformity of the available data and their resolution. Nevertheless, it is possible to make a coarse classification into the following two categories. (1) Cases where the existing evidence indicate average velocity contrast of 5 per cent or more that is persistent over distances of several tens of kilometres or more are labelled 'strong contrast'. (2) Cases where imaging studies indicate no contrast or possible mild contrasts that are likely to exist only in subsections of the zone and mixed with other sections of no contrast are labelled 'no-to-mild contrast'. We note that this latter category includes zones where there is evidence for two or more faults with reversed velocity contrasts, or reversal in the sense of contrast along strike and/or depth, which are expected to produce opposite effects on statistical results. This category also includes cases with limited imaging information, since it is more likely for a randomly chosen fault to have no-to-mild contrast.

In classifying the zones into one of the foregoing categories we use the highest available resolution results on bimaterial fault interfaces in the seismogenic zone (e.g. depth range of 3–15 km). The most informative signals are those associated with fault zone head waves that propagate along, and hence owe their existence to, velocity contrast interfaces (e.g. Ben-Zion 1989, 1990; Lewis *et al.* 2007; Zhao *et al.* 2010). In places where head waves studies have not been done we use, in this order, (i) results of reflection/refraction studies that focus on clarifying near-fault structures (e.g. Fuis *et al.* 2003) and (ii) local and regional tomographic studies (e.g. Eberhart-Phillips & Michael 1998; Tape *et al.* 2009). The classification of the zones to the different categories is summarized in Table 2 and can be described as follows.

Zones 1 and 2: No contrast based on the regional tomography of Tape *et al.* (2009). The website <http://www.data.scec.org/research/carltape/socalm16.html> gives various cross-sections of the 3-D image of Tape *et al.* (2009).

Zone 3: Possible mild contrast with faster NW side (Tape *et al.* 2009).

Zones 4, 7, 8, 13 and 14: No contrast (Tape *et al.* 2009).

Zone 5: Clear contrast with faster NE side based on seismic reflection imaging (Fuis *et al.* 2003).

Zone 9: Possible contrast with faster NE side (Tape *et al.* 2009).

Zone 10: No contrast to possible mild contrast with faster SW side (Tape *et al.* 2009).

Zone 11: Mild contrast with faster NE side based on local tomographic study (Scott *et al.* 1994).

Zone 12: Mild contrast with faster NE side (Tape *et al.* 2009).

Zone 15: Clear contrast with faster SW side (Tape *et al.* 2009).

Zone 42: Clear contrast with faster NE side based on head waves study (Ohlendorf *et al.* 2007) and regional tomography (Thurber *et al.* 2007).

Zone 43: Mild contrast with faster NE side (Ohlendorf *et al.* 2007; Thurber *et al.* 2007).

Zone 44: Mild contrast with faster SW side based on tomography studies (Michael & Eberhart-Phillips 1991; Thurber *et al.* 2007).

Zone 45: Mild average contrast with faster NE side based on local tomography (Michael & Eberhart-Phillips 1991) and head wave study (Zhao & Peng 2008).

Zone 46: No contrast based on tomography studies (Eberhart-Phillips & Michael 1998; Thurber *et al.* 2007).

Zone 47: No contrast to possible mild contrast with faster SW side (Eberhart-Phillips & Michael 1998).

Zone 48: Clear contrast with faster SW side based on head wave studies (McGuire & Ben-Zion 2005; Lewis *et al.* 2007) and local tomography (Thurber *et al.* 1997).

Zones 49 and 50: No to mild average contrast owing to seismicity in these zones on interfaces with opposite velocity contrasts (McGuire & Ben-Zion 2005).

Zone 51: Clear contrast with faster SW side based on head wave studies (Ben-Zion *et al.* 1992; Zhao *et al.* 2010) and local tomography (Eberhart-Phillips & Michael 1993; Thurber *et al.* 2006).

Zone 52: Minor average contrast based on the head-wave study of Zhao *et al.* (2010) and local tomography (Eberhart-Phillips & Michael 1993; Thurber *et al.* 2006).

3 METHODOLOGY

3.1 Background

Various studies demonstrated that large earthquakes can produce very asymmetric spatial seismicity patterns, with considerably

Table 2. Velocity contrast and expected short space-time asymmetry on the fault zones analysed in this study.

Contrast strength	Zone	Fault	Faster side	Preferred direction	Expected asymmetry	References
Strong, at least 5 per cent	5	SAF, Mojave	NE	NW	SE	Fuis *et al.* 2003
	15	Southern SAF	SW	SE	NW	Tape *et al.* 2009
	42	North Hayward	NE	SE	NW	Ohlendorf *et al.* 2007; Thurber *et al.* 2007
	48	SAF, creeping	SW	SE	NW	McGuire & Ben-Zion 2005; Lewis *et al.* 2007
	51	SAF, north Parkfield	SW	SE	NW	Michael & Eberhart-Phillips 1991; Ben-Zion *et al.* 1992; Zhao *et al.* 2010
No-to-mild, less than 5 per cent	1	Garlock		No contrast		Tape *et al.* 2009
	2					
	3	Garlock	NW	NE	SW	
	4	Lenwood–Lockhart		No contrast		
	7	Palos Verdes				
	8	Newport Inglewood (North)				
	9	Newport Inglewood (South)	NE	NW	SE	
	10	Ellsinore	SW	SE	NW	
	11	San Jacinto fault	NE	NW	SE	Scott *et al.* 1994
	12	Ellsinore	NE	NW	SE	Tape *et al.* 2009
	13	Cerro Prieto		No contrast		
	14	Imperial				
	43	South Hayward	NE	SE	NW	Ohlendorf *et al.* 2007; Thurber *et al.* 2007
	44	N. Calaveras	SW	SE	NW	Michael & Eberhart-Phillips 1991
	45	C. Calaveras	NE	NW	SE	Michael & Eberhart-Phillips 1991; Zhao & Peng 2008
	46	S. Calaveras		No contrast		Eberhart-Phillips & Michael (1998); Thurber *et al.* (2007)
	47	Sargent	SW	SE	NW	Eberhart-Phillips & Michael 1998
	49	SAF, creeping	SW	SE	NW	McGuire & Ben-Zion 2005
	50	SAF, creeping	SW	SE	NW	
	52	SAF, south Parkfield		Minor average contrast		Eberhart-Phillips & Michael 1993; Thurber *et al.* 2006; Zhao *et al.* 2010

enhanced teleseismic triggering in the predominant propagation direction of the parent large events (e.g. Hill & Prejean 2007). This is exemplified by studies associated with the 1992 Landers, CA, M7.3 earthquake, which induced remote seismicity to the NW over distances of several thousands of kilometres from the main rupture (Hill *et al.* 1993; Sturtevant *et al.* 1996; Gomberg *et al.* 2001). There is also evidence that large earthquakes can have on longer timescale clear asymmetric migration along major faults (e.g. Stein *et al.* 1997). However, there is little work on possible 'persistent' asymmetric seismicity patterns on short space–time scales following 'numerous' intermediate-to-small magnitude earthquakes in the same fault zone. In this work we perform such analysis by examining the symmetry properties of seismicity with respect to earlier events in a set of 25 fault zones. The analysis is focused on (i) revealing systematic spatio-temporal deviations of seismicity from purely random spatially symmetric patterns and (ii) relating these deviations to the local geological settings.

The main objects of our study are 'earthquake clusters'. In general, a cluster is defined as a group of earthquakes that occurred closer than usual to each other in time and space. A formal definition of closeness in space–time–energy domain will be given in Section 3.2; for prominent clusters this definition gives the same results as one's visual judgment. The most notable form of earthquake clustering is aftershock activity; accordingly, most of our analysis will be done within multiple aftershock sequences on given fault zones. At the same time, we would like to avoid entering a debate about whether or not each single event within our clusters is an aftershock. We thus adopt the following terminology. If event B occurred abnormally close to an earlier event A, we say that event A is 'the parent of' B, while B is called 'an offspring' (or child) of A. We will assume that each event can have only one parent; each event at the same time can be the parent to multiple children. Thus, a given event B can be a child to an earlier event A and the parent to later events C, D, etc. Since we consider only the projection of the hypocentres on the line that approximates the intersection of a fault with the Earth surface (fault line), our spatial analysis is purely 1-D. In the following we divide the spatial patterns of offspring events into (i) 'symmetric', if the events occur symmetrically in the along-strike direction with respect to their parents, (ii) 'positively asymmetric', if the offspring events occur primarily with a northward (NW or NE) offset relative to the parent earthquakes, or

(iii) 'negatively asymmetric', if the spatial distribution of children is biased in a southward (SW and SE) direction.

The research done so far on symmetry properties of seismicity on individual faults suggests (see e.g. Rubin & Gillard 2000; Rubin 2002; Schorlemmer & Ben-Zion 2008) that (1) asymmetric offspring distribution, when present, is a weak phenomenon, meaning that the total number of the offspring earthquakes with asymmetric properties is much smaller than the total regional seismic intensity; (2) the deviation from symmetry is a short-time effect, meaning that most of the earthquakes contributing to the asymmetry happen within the first days to weeks after the parent earthquake; (3) the results of statistical analysis may be contaminated by the *a priori* assignment of the parent–offspring relationships.

We try to overcome these difficulties by representing seismicity as a 'flow of clusters'. In this approach, we first identify significant earthquake clusters defined as the groups of earthquakes that happen unusually close to a parent earthquake in a space–time–energy domain. The asymmetry analysis is then done only for these predefined parent–children sequences. One key novelty of our analysis is in the first step: identifying statistically significant clustered sequences. There are several reliable approaches to earthquake cluster identification, starting from the pioneering works by Gardner & Knopoff (1974) and including later more formal methods (e.g. Reasenberg 1985; Davis & Frohlich 1991; Molchan & Dmitrieva 1992; Zhuang *et al.* 2002, 2004; Marsan & Lengline 2008). We use here a cluster identification technique by Zaliapin *et al.* (2008), which is based on a bimodal distribution of the parent–offspring distances in the time–space–energy domain and allows determination of the most probable parent for each earthquake (see Section 3.2). This approach is close in spirit to that of Zhuang *et al.* (2002, 2004) that assigns the most probable parent using a statistical inversion of the Epidemic Type Aftershock Sequence (ETAS) model. The main results of our study on spatial asymmetry properties of offspring events should not be very sensitive to a particular method of cluster detection.

3.2 Distance between earthquakes

3.2.1 Definition

A proper definition of the distance between earthquakes in space–time–energy domain is important for numerous problems, earthquake cluster identification being one of them. We adopt here the distance suggested by Baiesi & Paczuski (2004) for studying aftershock clustering. Below we define the distance in its general form that can be used for multidimensional spatial domains and takes into account possible fractal properties of the hypocentral distribution. In this study, we will only use a particular form of this definition, applied to 1-D spatial domain.

Consider an earthquake catalogue, where each event i is characterized by its occurrence time t_i, hypocentre (ϕ_i, $\lambda_{i,}$ d_i) and magnitude m_i. In cluster analysis, our primary goal is to detect for each earthquake j its possible parent, which is an earlier earthquake i that might have caused the occurrence of j. This triggering approach motivates us to consider a distance that is asymmetric in time. Specifically, the distance between earthquakes i and j is defined as

$$\eta_{ij} = \begin{cases} t_{ij}(r_{ij})^d 10^{-bm_i}, & t_{ij} > 0; \\ \infty, & t_{ij} \le 0. \end{cases} \quad (1)$$

Here $t_{ij} = t_j - t_i$ is the intercurrence time, which takes positive values if earthquake i happened before earthquake j and negative values otherwise; $r_{ij} \ge 0$ is the spatial distance between the earthquake hypocentres; and d is the (possibly fractal) dimension of the earthquake hypocentre distribution.

The definition (1) is motivated by the intuitive expectation that the value of η_{ij} should be small if there is a chance that earthquake j is related to earthquake i, and it should be large if there is no relationship between earthquakes i and j. To illustrate, consider a situation when $N(m)$ earthquakes with magnitude above m happen independently of each other in space and time and obey the Gutenberg–Richter relation $\log_{10}N(m) = a - bm$. Then the expected number of earthquakes having magnitude m within time t and distance r from any given earthquake is proportional to $tr^d 10^{-bm}$, which is an essential component of the definition (1). If the distance η_{ij} is abnormally small (smaller than most pair-wise distance within the catalogue), this means that earthquake j happens unusually close to i, and motivates one to consider i as a parent for j. We emphasize that this approach only reveals statistical, not causal, relationships between earthquakes.

In the next section we show that this intuitive reasoning is confirmed by analytical and simulation results, along with data analysis.

3.2.2 Space–time analysis

For our purposes it is sufficient to focus on the 'nearest-neighbour distance' (NND) between a given earthquake j and its nearest neighbour (parent) i. From now on, we will be working only with the NND using for it the same notation η_{ij} as that for the general distance in eq. (1), which should create no confusion. Zaliapin *et al.* (2008) studied the properties of the NND η_{ij} for a catalogue without clustering. Specifically, they considered a Poisson marked point process that is homogeneous in 2-D space, stationary in time and has magnitude marks that follow the Gutenberg–Richter distribution; we will refer to this process simply as a 'homogeneous Poisson process'. These authors demonstrated that for this process the NND η_{ij} has the Weibull distribution, which is the same distribution as that for the conventional NND in Euclidean spaces (Feller 1991). This result bridges between the cluster analysis in space–time–energy domains and the classical cluster results in multidimensional spaces, and thus provides a further justification for the use of the Baiesi-Paczuski distance in seismic cluster studies. The proposed cluster analysis is based on identifying significant deviations of the NND η_{ij} from the values expected in the absence of clustering.

Zaliapin *et al.* (2008) expanded a study of the scalar NND η to a more focused analysis of the joint distribution of the distance's spatial and temporal components. Specifically, they introduced the space and time NNDs normalized by the magnitude of the parent event.

$$T_{ij} = t_{ij}10^{-qbm_i}; \quad R_{ij} = (r_{ij})^d 10^{-pbm_i}; \quad q + p = 1. \quad (2)$$

It is readily seen that $\eta_{ij} = T_{ij}R_{ij}$, or $\log \eta_{ij} = \log T_{ij} + \log R_{ij}$. These authors demonstrated that for the homogeneous Poisson process introduced, the joint 2-D distribution of $\log T$ and $\log R$ is concentrated along the line $\log T + \log R = \text{const}$, illustrated in Fig. 3(a). In contrast, analysis of observed seismicity reveals a prominently bimodal joint distribution of ($\log T$, $\log R$). The latter distribution is illustrated in Fig. 3(b) for the data in southern CA, and in Figs 5(a), (c) and (e) for some individual fault zones. Here, the upper-right mode corresponds to a homogeneous Poisson process [*cf.* panel (a)], while the lower-left mode indicates the presence of a large subpopulation of events that are located significantly closer in time and space to their parents than expected in a Poisson process with no clustering. A more detailed analysis in Zaliapin

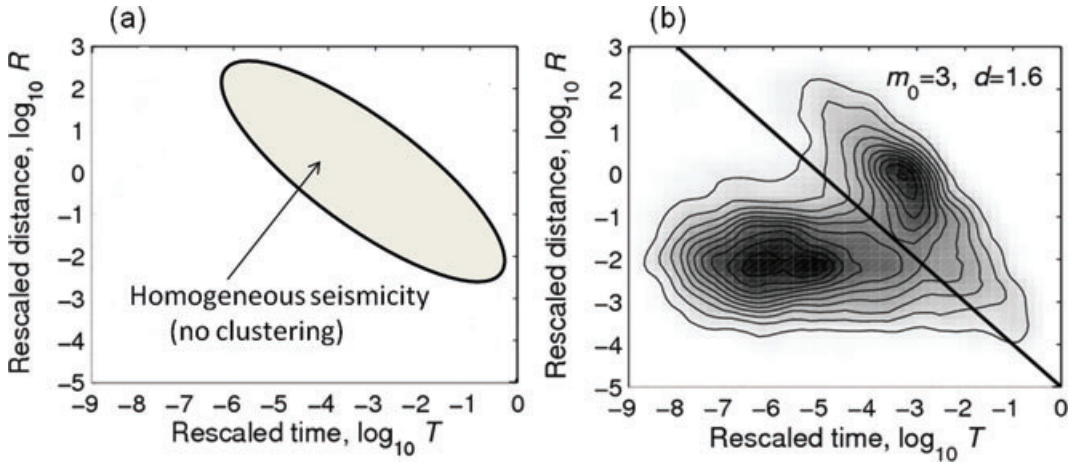

Figure 3. The joint 2-D distribution of the normalized space and time components of the nearest-neighbour distance η. (a) Theoretical prediction for a homogeneous Poisson process with no clustering. (b) Results for seismicity in southern California with magnitudes above $m_0 = 3.0$; the fractal dimension of epicentres is $d = 1.6$. The distribution in panel (b) shows a prominent bimodal structure comprising a homogeneous (main shocks) and clustered (aftershocks) parts. (After Zaliapin *et al.* 2008.)

et al. (2008), as well as basic intuition, suggest that those events are mainly comprising classical aftershocks, which are earthquakes that happen close in time and space to the parent event at a higher-than-normal intensity. This observation is further confirmed in this study.

In the following section, the 2-D joint distribution technique is used to identify significant earthquake clusters and to examine the along-strike symmetry properties of these clusters.

3.3 Earthquake clusters

The analysis of spatial asymmetry of seismicity is done within statistically significant clusters that are identified by the following procedure.

For each earthquake j in a catalogue, we identify its nearest neighbour (parent) i and the corresponding NND η_{ij}, using eq. (1) with $d = 1$ and r_{ij} equal to the along-strike (1-D) distance between events i and j. As a result, each earthquake is assigned a single parent (the nearest neighbour) and can be the parent for multiple offspring events. Next, we analyse the 2-D joint distribution of the normalized time (T) and space (R) components of the NND. To make the results directly comparable among parent events of different magnitudes, we further normalize the spatial distance R by the rupture length L_m of the parent event with magnitude m. For crack-like events with circular rupture areas, the rupture length is given (e.g. Ben-Zion 2008) by

$$L_m \approx 0.0152 \times 10^{0.42m}.$$

This leads to the following definition of the normalized distance:

$$R_{ij} = \frac{r_{ij} 10^{-pbm_i}}{0.0152}, \tag{3}$$

with $p = 0.42$. The definition (3) differs from the general definition (2) only by the constant 0.0152.

Notably, each of the 25 catalogues considered in this study has a prominently bimodal 2-D distribution of its space–time components (this is illustrated in Figs 5a, c and e for three fault zones), consistent with the earlier results of Zaliapin *et al.* (2008). As discussed, the clustered part of seismicity is located within the lower-left mode of the bimodal distribution; this property helps to identify the clustered events for further symmetry analysis. A given event j is called *clustered* if it happened within a given normalized time and a given normalized distance from its parent, and has magnitude lower than that of the parent. Formally, event j is called clustered if

$$R_{ij} < R_0, \quad T_{ij} < T_0 \quad \text{and} \quad m_j < m_i. \tag{4}$$

The values of the thresholds R_0 and T_0 are discussed further later. Only events satisfying conditions (4) are considered for future analysis.

All clustered events can be decomposed into separate clusters such that each event in a given cluster is a descendant (i.e. child, child of child, etc.) of the cluster's first event (see Fig. 4). In the following sections we analyse the symmetry properties of events in each cluster relative to their parents.

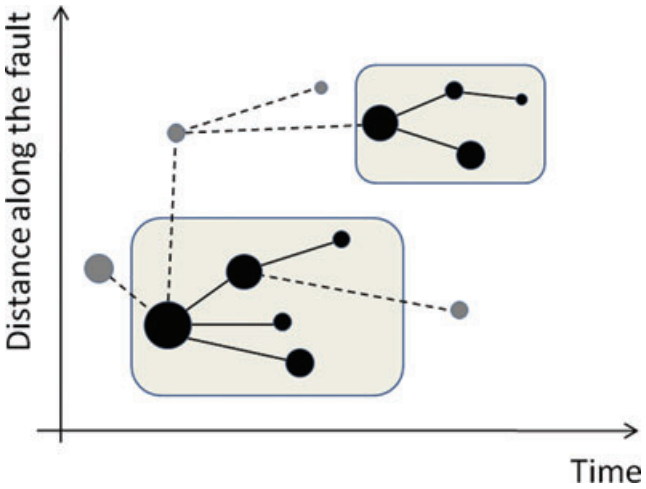

Figure 4. An illustration of cluster definition. Each event in the catalogue is connected to its nearest neighbour (parent) as indicated by the solid and dashed links. The solid links represent clustered events (short nearest-neighbour distance) based on the definition (4), while the dashed links represent un-clustered events (long nearest-neighbour distance). Only solid links are considered in the analysis. The catalogue in this plot has two clusters, shown by black circles, enclosed by grey shadows. The un-clustered events are shown by light circlers.

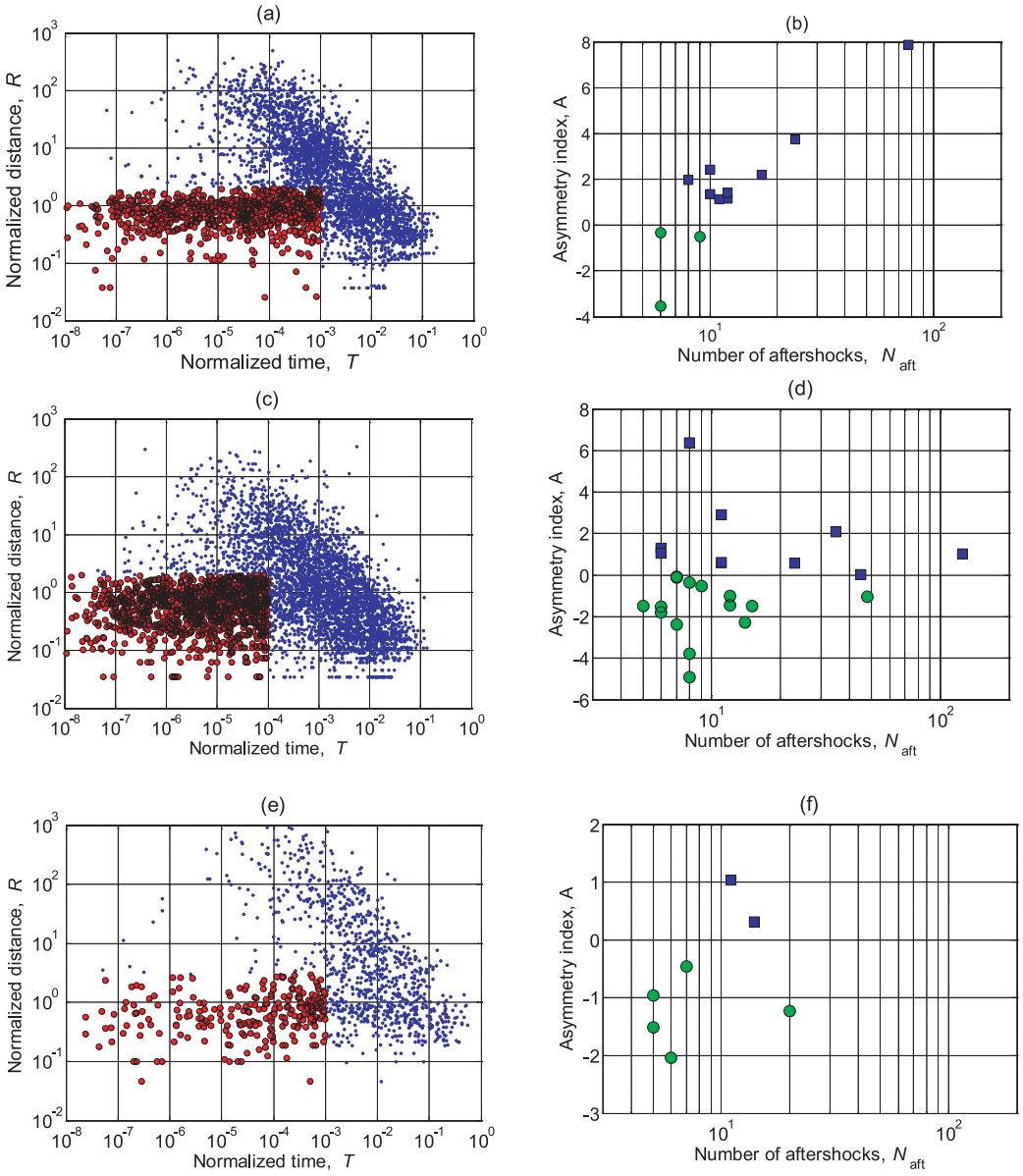

Figure 5. Illustration of asymmetry analysis. (a, c and e): Joint distribution of space and time components of the nearest-neighbour distance η_{ij} . (b, d and f): Values of the asymmetry index as a function of the number of events in the cluster. (a and b): Zone 51 (SAF, Parkfield), NW asymmetry; (c and d): Zone 49 (SAF, creeping), symmetric seismicity; (e and f): Zone 5 (SAF, Mojave), SE asymmetry. Filled red circles in panels (a, c and e) indicate clustered events used to compute asymmetry indices shown in panels (b, d and f). Blue squares in panels (b, d and f) indicate positive (northward) values of the asymmetry index, green circles—negative (southward) values. Note a prominent bi-modal distribution in panels (a, c and e), used to identify clustered events.

3.4 Evaluating along-strike asymmetry of seismicity

We consider two approaches to examine along-strike symmetry. Both approaches start with calculating the along-strike offsets of the clustered events with respect to their parents. The first approach involves detailed analysis over short space–time scales; it assigns asymmetry index to each cluster, uses these to determine combined asymmetry index of all clusters in each fault zone and describes the results in terms of northward and southward offsets. The second approach involves somewhat coarser analysis over broader ranges of time–space scales; it averages the individual offspring offsets within all fault zones with and without strong contrasts, and describes the stacked along-strike asymmetries in terms of the preferred and opposite directions. The two approaches provide complementary information about symmetry properties of seismicity.

In the first approach, for each child-earthquake j within a cluster, we define S_{ij} as the 'signed normalized distance' from this earthquake to its parent i. The absolute value of S_{ij} is R_{ij} defined by (3); the sign is positive if the child has a northward (NW or NE) spatial offset with respect to the parent and negative if the child has a southward (SW or SE) offset. The degree of asymmetry within a given earthquake cluster k is measured by the asymmetry index A_k.

$$A_k = \sqrt{n}\frac{\mathrm{mean}(S)}{\mathrm{st.dev}(S)} = \frac{\sum_{j=1}^{n} S_{ij}}{\sqrt{\sum_{j=1}^{n}\left(S_{ij} - \frac{1}{n}\sum_{j=1}^{n} S_{ij}\right)^2}}, \qquad (5)$$

where $S = \{S_{ij}\}, j = 1,\ldots,n$ is the sample that consists of all signed spatial distances in the cluster k. Using the distances normalized by the parent's rupture length (see eq. (3)) ensures that the results are directly comparable among the parent events of different magnitude.

The asymmetry index A_k of a cluster on a finite fault can be misleading if the parent is located near the edge of the fault. In this case, most of the offspring events will necessarily be offset towards the middle of the fault, resulting in a biased value of the asymmetry index A. To avoid this problem, we consider only offspring events inside a symmetric strip within the fault zone around the parent location. As example, if the coordinate of a parent is $x = 1$ km, then only children with coordinates from 0 to 2 km are considered in computing the asymmetry index.

It is known from statistics (e.g. Venables & Ripley 2002) that if the distances S_{ij} are normally distributed with zero mean and arbitrary variance then the index A has the Student distribution. Moreover, for an arbitrary distribution of individual distances S_{ij} having a finite variance, the distribution of A converges for large n to the Normal distribution with a unit variance (and probably non-zero mean). These facts help in evaluating the significance of the values of the asymmetry index. Specifically, if a clustered sequence is symmetric and the signed distances S_{ij} have zero mean, the asymmetry index value should lie close to zero, within the error margins suggested by the standard Normal distribution. If a clustered sequence is asymmetric and the signed distances S_{ij} have non-zero mean, the value of the asymmetry index should deviate significantly from zero, falling outside of the error margins suggested by the standard Normal distribution. In summary, significant positive values of the index imply that there exists a statistically significant northward offset of the clustered events relative to their parents, and significant negative values imply that there exists a southward offset. Values around zero suggest that the sequence is not statistically distinguishable from a symmetric one. In the analysis of data, we use the empirical distribution of the index values (rather than theoretical Student or Normal statistics) to determine the significance of the asymmetry index.

The second approach to symmetry analysis attempts to consider broader ranges of space–time scales and simplify the interpretation of results. Specifically, we introduce the signed distance W_{ij} such that $|W_{ij}| = R_{ij}$, with R_{ij} defined by eq. (3). For the zones with mild and strong contrasts, we use a sign convention related to the preferred propagation direction predicted from the local velocity contrast (see Table 2). In these zones, W_{ij} takes positive or negative values for offspring's offset in the preferred or the opposite along-strike directions, respectively. The asymmetry of a given group of children is characterized by the average value of W_{ij}, which is measured in parent rupture lengths. Hence, an excess of offspring events in the preferred along-strike direction would correspond to positive average values of W, and vice versa. For the no contrast zones, positive (negative) values correspond to the southward (northward) offset. To enhance the statistical significance of our results in various space–time scales, we stack the values of W_{ij} obtained for the group of faults with strong contrast, and those obtained for the faults with no to mild contrast.

4 DATA ANALYSIS

As mentioned, we analyse the symmetry properties of earthquake clusters in 25 fault zones defined by Powers & Jordan (2010), which are shown in Fig. 2 and described in Table 1. In each zone, we identify significant clusters following the procedure of Section 3.2 and examine both the cluster asymmetry A and earthquake asymmetry W. Section 4.1 focuses on the cluster asymmetry measure A for each examined zone. Section 4.2 considers the event offset W along-strike, averaged over all events within (i) strong and (ii) no-to-mild contrast zones.

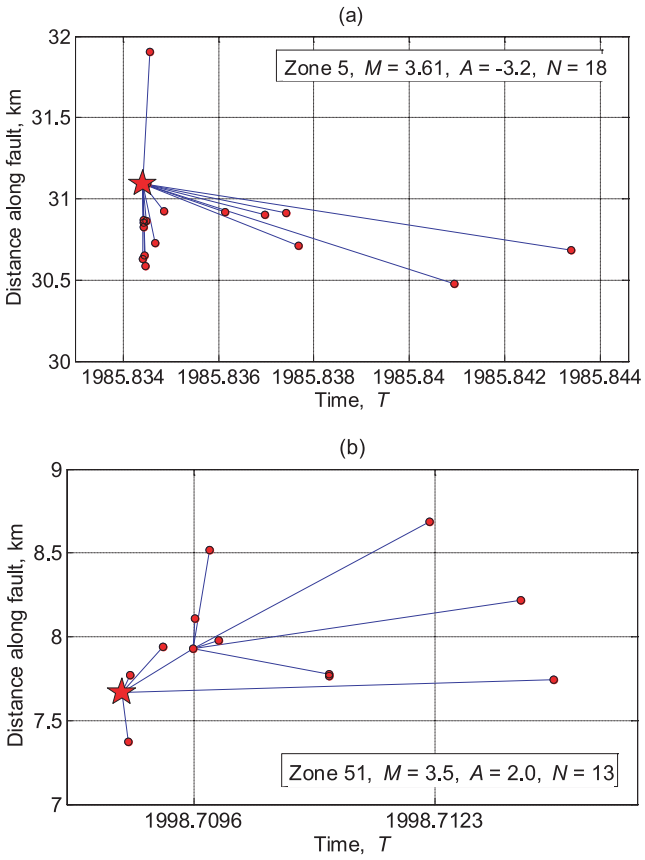

Figure 6. Examples of sequences with notable asymmetries in zones 5 (panel a) and 48 (panel b). Star indicates the cluster's parent (main shock). Filled circles connected to the parent indicate clustered events (aftershocks). The main shock magnitudes, value of the asymmetry index A, and the number N of events in the sequence are indicated in the panels.

4.1 Zonal asymmetry index

We analyse here symmetry properties within each fault zone using the cluster asymmetry index of eq. (5). Recall that for this asymmetry index, positive (negative) values correspond to northward (southward) offset of children with respect to the parent. Fig. 5 illustrates the joint distribution of the space and time components of the NND η (panels a, c and e) and the values of the asymmetry index A_k as a function of the number of events in a cluster (panels b, d and f). The results are presented for three zones: Zone 51 (panels a and b) for the section of SAF just NW of Parkfield shows significant positive (NW) asymmetry; Zone 49 (panels c and d) for a portion of the creeping section of the SAF shows no significant asymmetry; and Zone 5 (panels e and f) for the Mojave section of the SAF shows significant negative (SE) asymmetry. Fig. 6 provides a detailed illustration of two clusters (in the original time–space coordinates) from Zones 5 and 48 with notable SE and NW asymmetries, respectively. The opposite senses of asymmetries exhibited by these sequences are consistent with our overall statistical findings discussed later. Nevertheless, one cannot make meaningful claims based on the results associated with these or any other individual sequences; Fig. 6 merely serves to illustrate aftershock asymmetry.

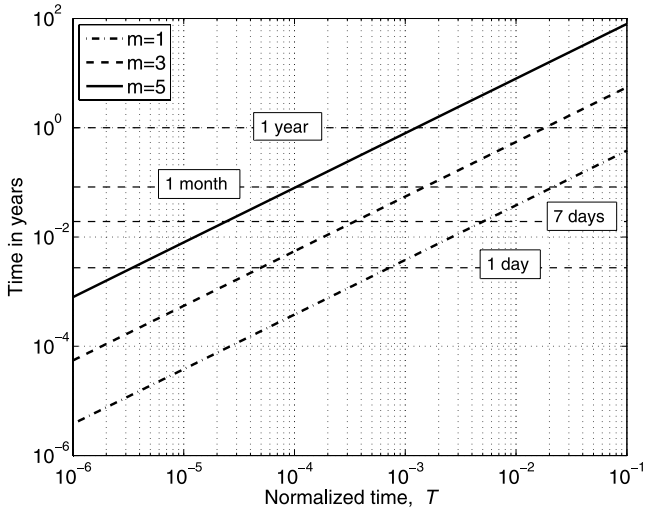

Figure 7. Correspondence between the normalized time T (x-axis) used in the asymmetry analysis and time in years (y-axis) for earthquakes of different magnitudes, $m = 1$, 3 and 5. Horizontal lines indicate times of 1 d, 7 d, 1 month and 1 yr.

An important observation is that in all 25 zones, the 2-D distribution of space and time components of the NND is prominently bimodal (e.g. Fig. 5, panels a, c and e). This provides an objective guidance for separating clustered sequences from more homogeneous seismicity. Still, there is some remaining ambiguity in setting up specific thresholds to identify clusters. To reduce this ambiguity, we have repeated our analysis in each fault zone with alternative definitions of clustered sequences, varying the time and space thresholds T_0 and R_0 over broad ranges. We also varied the minimal magnitude of main shocks considered in the analysis. Specifically, the normalized time threshold T_0 has been varied from 10^{-6} to 10^{-2}, which for a magnitude $m = 3$ event corresponds to the interval from 30 s to about 1 yr (see Fig. 7); the normalized distance threshold R_0 has been varied from 1 to 3 main shock rupture lengths; and the minimal magnitude of main shocks has been varied from 1.5 to 3. This has resulted in 1968 distinct triplets of parameters. The asymmetry index has been computed for each triplet in each of the 25 fault zones. Table 1 lists the number of parents (being also the number of clusters) computed with $T_0 = 10^{-2}$, $R_0 = 3$ and minimal magnitude of 1.5. This forms the data set of clusters analysed in this study (i.e. each version of our analysis uses a subset of these clusters). We emphasize that the 1968 versions of analysis 'may not' be considered as independent tests for the same zone; the cluster sets for different versions are significantly overlapped. Notably, the large clusters associated with large-magnitude parents are present in almost all versions.

Recall that the asymmetry index A of eq. (5) assesses the asymmetry of a single cluster. To characterize the overall asymmetry of seismicity in a given zone, we use a weighted average of the values A_k from all individual clusters. It should be noted that most of the clusters consist of only a couple of events, and using them in evaluating seismic distribution asymmetry is inefficient. We therefore use only clusters with more than five events, meaning that the weight of a cluster with less than five events is set to zero. The weights of the other clusters are made proportional to the number of events within a cluster. Finally, the zonal asymmetry index A is computed as

$$A = \frac{\sum A_k N_k}{\sum N_k}, \tag{6}$$

where A_k is the asymmetry index for cluster k comprising N_k events and the summation is taken over all clusters with more than five events. Table 1 lists for each zone the number C_5 of clusters with more than five events and the average number $<L_5>$ of events in the clusters with more than five events.

Fig. 8 shows histograms of the asymmetry index in three zones with different asymmetry properties. Zone 51 (panel a) exhibits prominent NW (positive) asymmetry; zone 49 (panel b) shows no (or probably a very weak NW) asymmetry; and zone 5 (panel c) shows significant SE (negative) asymmetry. Each of these histograms clearly reflects the symmetry property of a given zone. As indicated in Table 2, the analysis results for these three zones are in accordance with the expectations based on the theoretical results on bimaterial ruptures and the available information on the velocity contrasts across the faults.

The distribution of asymmetry indices in all 25 zones is summarized in Fig. 9. For each zone we show the index mean (solid circle) and error bars that span the range between the 5 per cent and 95 per cent empirical percentiles of the asymmetry index sample (i.e. they mark a 'prediction interval' for the index values, not 'confidence interval' for the mean). Hence, the middle 90 per cent (or 1771 out of 1968) of asymmetry indices lie within the error bars. Fig. 9 orders the zones according to our assessment of the degree of velocity contrast (see Table 2): zones 5, 15, 42, 48 and 51 have strong velocity contrasts (shown by red) and are followed by the other zones which have no-to-mild contrast (shown by blue).

To roughly assess the significance of the asymmetry index, we show in Fig. 9 by a horizontal yellow bar the range between the empirical 10 per cent and 90 per cent percentiles of the A-values computed only within the 20 no-to-mild contrast zones. Zones where the average asymmetry index is lying outside of this range can be considered significantly asymmetric. We emphasize that we are not trying to define a formal significance criterion for this problem, which is a hard task mainly due to serious dependence among the A-values in the same zone, but rather suggest the empirical bounds as a convenient visual tool. One can readily see that 'all' zones with strong velocity contrast have asymmetry indices outside of the empirical bounds; while most of the zones with no-to-mild contrast have asymmetry index within the bounds.

To further illustrate the difference between the asymmetry properties of the two categories of zones, we show in Fig. 10 the histograms of amplitudes $|A|$ of the asymmetry indices in 'all' strong contrast zones (panel a) and in 'all' no-to-mild contrast zones (panel b). The difference between the two distributions is readily seen and is formally confirmed by any relevant statistical test, for example, Kruskal-Wallis or ANOVA (Venables & Ripley 2002).

4.2 Average distance to parent

Here we calculate the average normalized signed distance W from offspring to parent events, measured along the fault line. We compare the values of W averaged over all offspring within all strong versus all no-to-mild contrast zones for different parent magnitudes and within different spatio-temporal neighbourhoods of the parents. The results are summarized in Fig. 11, which shows the average values of W, together with the corresponding 95 per cent confidence intervals, as a function of the offspring time threshold T_0.

Figs 11(a) and (b) present the results for parent magnitudes $m \geq 3$ (panel a) and $m < 3$ (panel b), using spatially close offspring events that are within one parent rupture distance along strike from the parent ($R_0 = 1$). The time threshold T_0 is varied from 10^{-7} to 10^{0}; for a magnitude $m = 3$ event this corresponds to the interval from

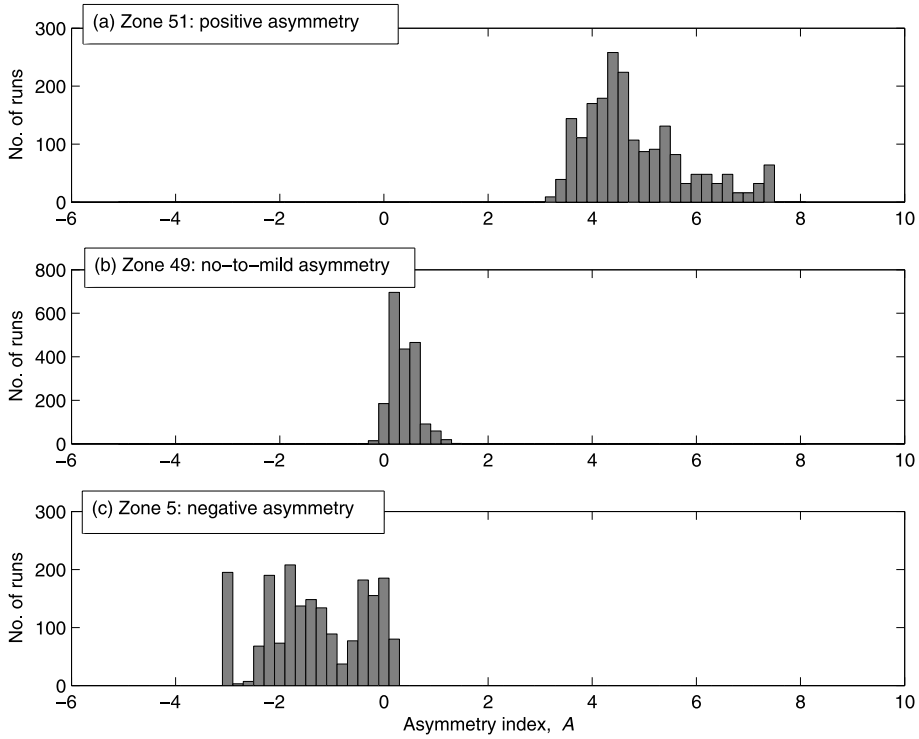

Figure 8. Histograms of asymmetry index for 1968 versions of offspring definition (see Section 4.1). (a) Zone 51 (SAF, Parkfield), NW (positive) asymmetry; (b) Zone 49 (SAF, creeping), symmetric triggering (probably mild positive asymmetry) and (c) Zone 5 (SAF, Mojave), SE (negative) asymmetry.

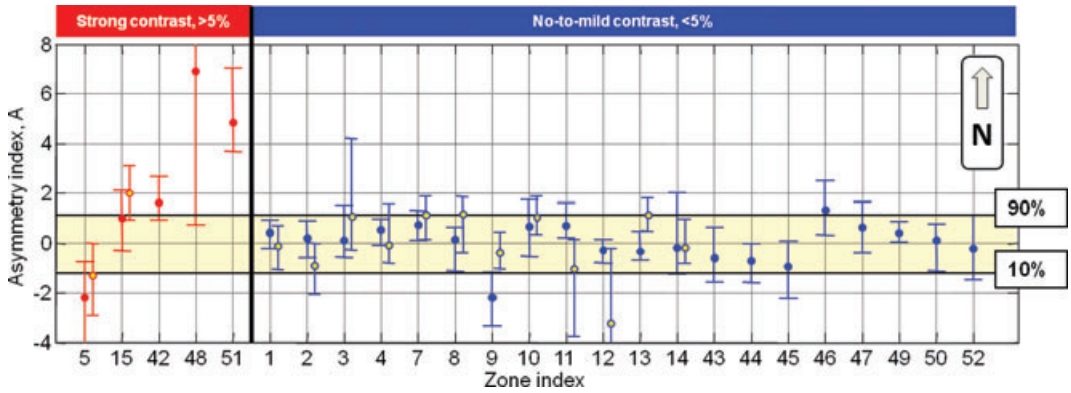

Figure 9. Asymmetry results for the 25 fault zones considered in the study. Dots depict the mean values of the zonal asymmetry index A; the zones denoted by indices are shown in Fig. 2 and discussed in Tables 1 and 2. The error bars show the range between 5 per cent and 95 per cent empirical percentiles of the asymmetry index distribution for 1968 estimations with different parameter values (see Section 4.1 for details). Horizontal yellow bar marks the range between 10 per cent and 90 per cent empirical quantiles of the asymmetry index distribution within the 20 no-to-mild contrast zones, and provides a guide for assessing the significance of the asymmetry. Red colour corresponds to the strong contrast zones (zones 5, 15, 42, 48 and 51), blue to no-to-mild contrast zones. Filled and empty dots of the same colour correspond, respectively, to the catalogues of Shearer *et al.* (2005) and Hauksson & Shearer (2005) in southern California. For northern California faults, the relocated catalogue of Ellsworth *et al.* (2000) is used. Positive values correspond to northward asymmetry (NE or NW); negative values correspond to southward asymmetry (SE or SW).

3 min to the complete duration of the catalogue (*cf.* Fig. 7). Within no-to-mild contrast zones (blue dashed lines) the average signed distances are not significantly different from 0, indicating a statistically symmetric distribution of the offspring events. However, within the strong contrast zones (red solid lines) the average signed distances are in various places significantly negative, indicating an opposite along-strike offset of the events. For larger parent magnitudes ($m \geq 3$, panel a), the asymmetry is seen at all time thresholds with prominently high $W < -0.4$ for early events (smaller values of T_0). We emphasize that we restrict this analysis to offspring events within one parent rupture length, so a uniform distribution of events exclusively within the opposite direction corresponds to $W = -0.5$. For smaller parent magnitudes ($m < 3$, panel b), the result is qualitatively similar, although the average amplitudes of W are lower and the asymmetry is seen only for early aftershocks, $10^{-7} \leq T_0 \leq 10^{-4}$; for a magnitude $m = 3$ event this corresponds to the interval from 3 min to 2 d (*cf.* Fig. 7).

Fig. 11(c) focuses on spatially distant offsprings—within 2–10 parent rupture lengths and small parent magnitudes ($m < 3$). For no-to-mild contrast zones (blue dashed line), the average signed distance is still not significantly different from 0. However, for the strong contrast zones (red solid line) we see a clear opposite effect

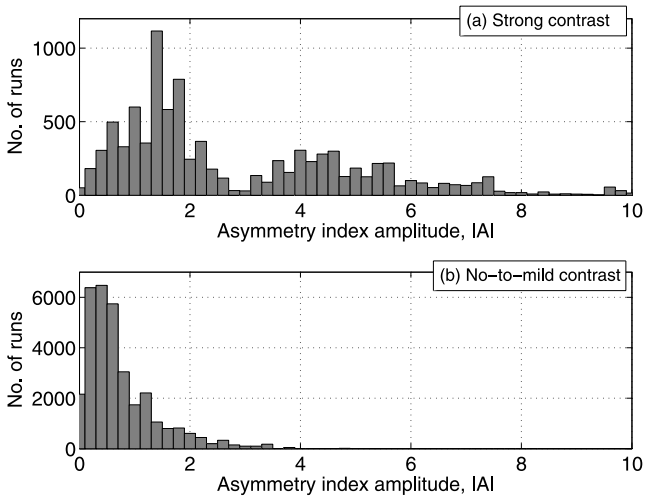

Figure 10. Comparison between seismic symmetry properties within strong and no-to-mild contrast zones. (a) Histogram of the amplitude of the asymmetry index A for the strong contrast zones. (b) Histogram for the no-to-mild contrast zones. The difference in the two distributions is clearly visible. Panel (a) shows only the left part of the entire distribution, which includes values above 10.

to that observed in Figs 11(a) and (b): the average signed distance is significantly positive with values as high as $W = 4.5$. This indicates an excess of the offspring events within the preferred along-strike direction. We note that a uniform distribution of children exclusively within the preferred direction would correspond to $W = 6$. Significantly positive values are seen for $10^{-3} \leq T_0 \leq 10^{-2}$; for a magnitude $m = 3$ event this corresponds to the interval from 20 to 200 d (*cf.* Fig. 7). A similar analysis for larger magnitudes is compromised by the fact that 2–10 parent rupture lengths area typically exceeds the fault size.

To summarize, within the no-to-mild contrast zones the spatial along-strike distribution of offspring events is symmetric with respect to the parents at all examined space–time scales. On the other hand, within the strong contrast zones one clearly sees statistically significant asymmetry effects, which vary with time and space distances to the parents. Specifically, (i) the early close offspring events tend to occur with the opposite along-strike offset with respect to the parents—this effect is seen within minutes to days and within one parent rupture length zone; (ii) the later and more distant offspring events tend to occur with the preferred along-strike offset with respect to the parents—this effect is very prominent after tens of days and outside of the two parent rupture length zone.

4.3 Alternative analyses

In addition to the main version of symmetry analysis involving the index A, we have tested several alternatives. First, we defined the asymmetry index within a cluster as a simple mean, $A = \text{mean}(S)$, without the normalization of eq. (5). Second, we defined the asymmetry index for a given zone as a simple average of asymmetry indices within individual clusters, without the weights of eq. (6). This means that altogether we have considered two definitions of the asymmetry index within a cluster and two definitions of the asymmetry index in a zone. These result in four alternative versions of computing the final asymmetry index in a given zone. We present in the paper only the results with normalized and weighted definitions described by eqs (5) and (6). The other three versions of analysis give qualitatively similar results, with all zones that have strong contrast showing significant asymmetry. Furthermore, in each of the four versions of analysis we changed the threshold for the minimal number of events in a cluster from 2 to 10 and found no significant differences with the results of the main analysis (threshold of five events) reported in Section 4.1. To analyse the effect of secondary offspring events, we repeated the analyses of Sections 4.1 and 4.2 using only the direct offspring for a given parent. The results are quantitatively close to those presented in the paper.

5 INTERPRETATION OF RESULTS

We now compare the results of the purely statistical analysis of Section 4 with the theoretical expectations associated with the degree and sense of velocity contrast across each of the examined fault zones. The information on the velocity contrast profiles is taken from different sources; see Section 2.2 and Table 2.

5.1 Strong contrast zones

Notably, all five zones with a well-established strong velocity contrast (zones 5, 15, 42, 48 and 51) exhibit strong asymmetry in the directions consistent with the theoretical predictions based on the reported velocity contrasts. For instance, in zone 48 (creeping section of the SAF south of Hollister) and zone 51 (creeping SAF section just north of Parkfield), the strong NW asymmetry on short space–time scales associated with the significantly positive index A (Section 4.1) is consistent with seismic imaging of the velocity contrast based on head waves and local tomography (e.g. Ben-Zion *et al.* 1992; McGuire & Ben-Zion 2005; Thurber *et al.* 2006). The results in zone 48 of Section 4.1 are also consistent with similar findings of Rubin & Gillard (2000) and seismic imaging results on asymmetric rock damage (Lewis *et al.* 2007). In zone 5 (the Mojave section of the SAF), the SE asymmetry of the index A is consistent with evidence (e.g. Fuis *et al.* 2001) for a 'reversed' velocity contrast compared to the central section of the SAF (with the NE block having faster velocity) and field observations of asymmetric rock damage in that section (Dor *et al.* 2006a,b). The stacked results for all the zones with strong velocity contrast associated with the index W (Section 4.2) are consistent with the patterns on short space–time scales of Section 4.1, and in addition show reversed patterns that are expected on larger space–time scales (more offspring events in the preferred direction).

5.2 No-to-mild contrast zones

Most of the zones in this category show indeed no-to-mild values of the asymmetry index A. In particular, it is interesting to note the lack of asymmetry in zone 52 (creeping SAF section just south of Parkfield) that stands in marked contrast with the strong asymmetry in the neighbouring zone 51 north of Parkfield. The lack of asymmetry in zone 52 is consistent with the near zero average velocity contrast in that section based on high-resolution head waves and local tomography imaging studies (Eberhart-Phillips & Michael 1993; Thurber *et al.* 2006; Zhao *et al.* 2010). We discuss later, one by one, zones that show significant asymmetry for at least one catalogue. Notably, only two of the 20 no-to-mild contrast zones show behaviour that is inconsistent with the velocity profile prediction of Table 2. The stacked values of the asymmetry index W for all zones with no-to-mild velocity contrast are statistically indistinguishable from zero for all examined parent magnitudes and spatio-temporal scales.

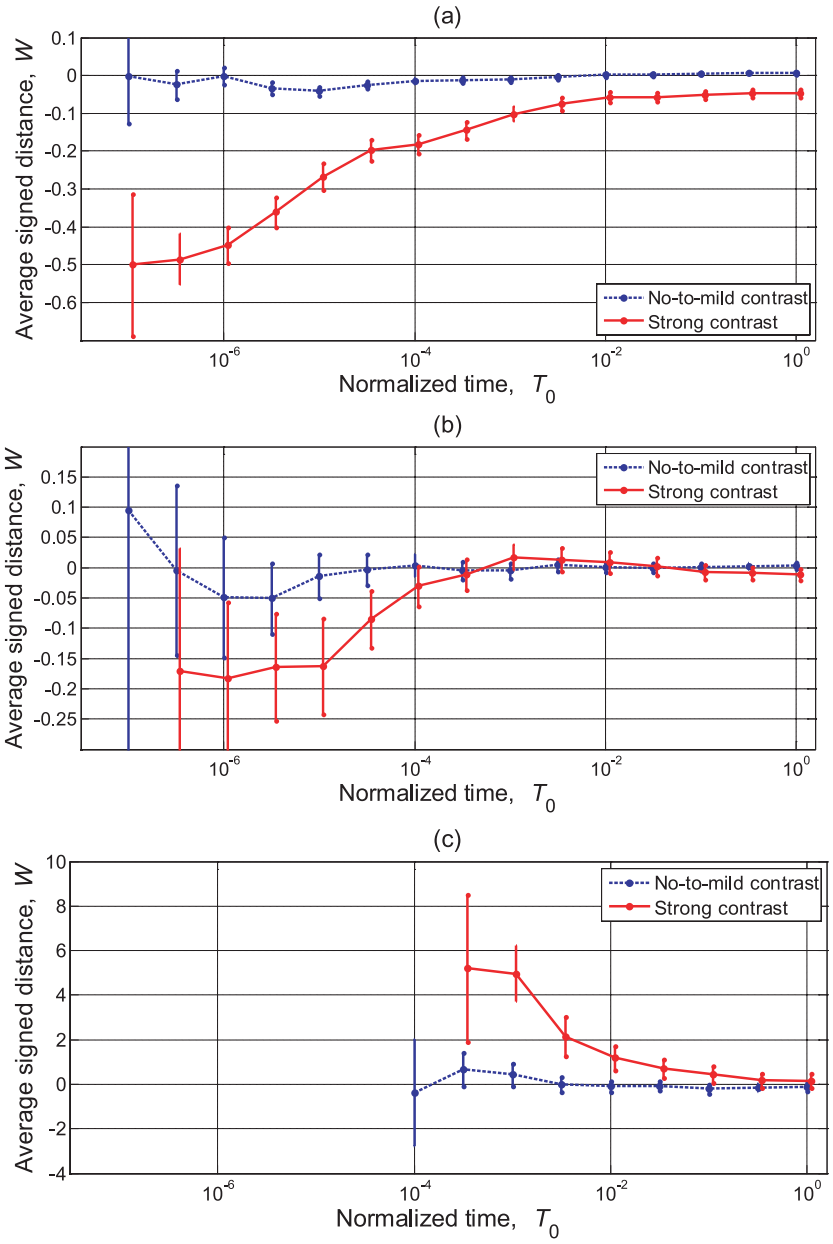

Figure 11. Average signed normalized distance W_{ij} for no-to-mild (blue dashed line) and strong (red solid line) contrast zones for offspring events within normalized time T_0 from the parents. Positive (negative) values of W correspond to the preferred (opposite) along-strike direction. (a) Parents with magnitude $m \geq 3$ and close offsprings—within one parent rupture distance. (b) Parents with magnitude $m < 3$ and close offsprings—within one parent rupture distance. (c) Parents with magnitude $m < 3$ and offsprings within 2 to 10 parent rupture distances.

Zone 3 (western section of the Garlock fault) shows a somewhat NE asymmetry when using the Hauksson & Shearer (2005) catalogue. This is not consistent with a mild velocity contrast with faster NW side, based on the regional tomography results of Tape *et al.* (2009) at depths around 5 km which corresponds to the average seismic depth in this zone. A number of mechanisms may produce a competing effect to the velocity contrast that may be responsible for the discrepancy. Examples include fault curvature or dip, permeability contrast around the rupture zone with reserved sense from that of the elastic contrast (Rudnicki & Rice 2006; Dunham & Rice 2008), persistent stress concentration at the NE portion of zone 3, perhaps due to proximity to faults of the Eastern CA shear zone, or another source that produces enhanced hypocentre production to the NE. It is also possible that there exists a local velocity contrast across the fault with faster SE side that is not resolved by the regional tomography imaging.

Zone 9 (south Newport Inglewood) shows significant SE asymmetry for the Shearer *et al.* (2005) catalogue, which is consistent with a velocity contrast with faster NE side at the depth of 10 km reported by Tape *et al.* (2009). The average seismicity depth in this zone is 9.82 km.

Zone 11 (San Jacinto) shows a tendency to SE asymmetry for the Hauksson & Shearer (2005) catalogue that is consistent with seismic imaging of the velocity contrast in this region (Scott *et al.* 1994) and asymmetric rock damage based on trapped waves (Lewis *et al.* 2005) and geological data (Dor *et al.* 2006a; Wechsler *et al.* 2009).

Zone 12 (Ellsinore) shows SE asymmetry for the Hauksson & Shearer (2005) catalogue that is consistent with the velocity profile

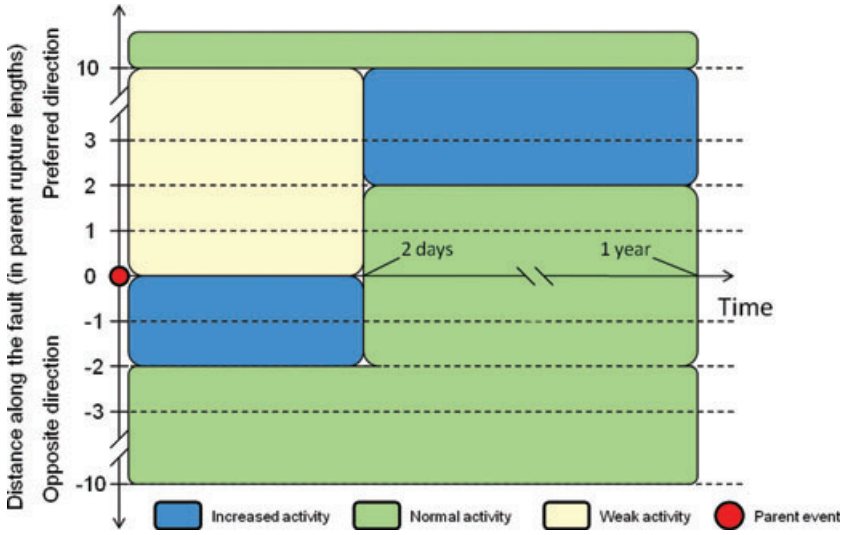

Figure 12. A schematic illustration of expected variations in the spatio-temporal distribution of offspring earthquakes on bimaterial faults. The parent event is located at the origin (red dot). The time and space scales are approximate. The indicated changes of the offspring intensity are multiplicatively applied to a spatially symmetric cluster intensity model that takes into account the intensity decay further away from the parent in space and time. See a detailed discussion in Section 6.

of Tape *et al.* (2009) at the depth of 10 km. The average seismicity depth in this zone is 9.91 km.

Zone 46 (southern Calaveras) exhibits a possible tendency to NW asymmetry. This may, perhaps, reflect persistent high stress concentration and hypocentres production at the SE end of the zone near the intersection with the SAF, or one of the other mechanisms noted for zone 3.

6 DISCUSSION

Rupture propagation along faults is expected generally to be affected by the structural properties of the fault, the initial stress distribution on the fault and the dynamical stresses produced by the rupture. However, the relevant information on the fault properties and stress conditions, as well as clear predictions that can be tested with seismic data, are typically not available. The hypothesis that earthquake ruptures on bimaterial faults separating different elastic solids have a preferred propagation direction (e.g. Ben-Zion 2001 and references therein) is one of the clearest predictions to emerge from theoretical models of dynamic rupture. A persistent statistical bias in the directivity of earthquakes on large bimaterial faults, which tend to be the sites of the largest earthquakes in a region, can have profound effects on the distribution of strong ground motion and expected damage patterns associated with these faults.

To facilitate the discussion, we schematically summarize in Fig. 12 the structure of a parent–offspring cluster suggested by bimaterial ruptures with a preferred propagation direction (e.g. Ben-Zion & Andrews 1998; Ampuero & Ben-Zion 2008; Brietzke *et al.* 2009) and confirmed by this study. The vertical axis corresponds to the along-strike line with positive values assigned to the preferred direction. The horizontal axis represents time. The parent event (red dot) is located at the origin and the expected spatio-temporal intensity of the children is indicated by different colours. Blue zones represent increased offspring activity, the green zones represent normal average activity and the yellow zone represents weak sporadic activity. The space and time marks are approximate and intended to provide a simple guidance rather than precise bounds. The actual offspring intensity within each indicated zone is not uniform; it decays in time and space further away from the parent. The zones in Fig. 12 should be considered as multiplicative filters applied to any reasonable spatially symmetric intensity model of a seismic cluster. The figure illustrates the following effects. Immediately after the occurrence of a parent earthquake, offspring events are enhanced in the negative direction very close to the parent (blue zone over 1–2 parent rupture lengths). At this time, essentially no events occur in the preferred direction since the sites of potential offsprings have been merged with the main rupture, as well as in the opposite direction far away from the parent. This asymmetry fades off with time and after a few days the spatial offspring distribution becomes symmetric in the vicinity of the parent's location (green zone). On a similar timescale, another prominent asymmetry develops at larger distances from the parent in the positive direction (blue zone over 2–3 to 10 parent rupture lengths). This excess of offspring events is generated by increased moment release and seismic radiation in the preferred direction.

On natural faults, the dynamic bimaterial effects leading to the preferred propagation direction (and the effects illustrated in Figs 1 and 12) will compete with numerous other effects. Examples include various types of frictional properties (e.g. Harris & Day 1997; Ben-Zion & Huang 2002; Rubin & Ampuero 2007; Ampuero & Ben-Zion 2008), stress heterogeneities (e.g. Ben-Zion & Andrews 1998; Ampuero & Ben-Zion 2008; Brietzke *et al.* 2009) and additional structural components such as low velocity fault zone layers (e.g. Harris & Day 1997; Ben-Zion & Huang 2002; Brietzke & Ben-Zion 2006) and small-scale granular zones with different permeability (Rudnicki & Rice 2006; Dunham & Rice 2008). These and other ingredients can lead to deviations from the basic theoretical predictions and a mixture of outcomes. Nevertheless, the large parameter-space study associated with all the available theoretical results indicates that bimaterial ruptures tend to evolve with propagation distance for wide ranges of conditions towards pulses (Fig. 1) that propagate predominately in the preferred direction (e.g. Shi & Ben-Zion 2006; Ampuero & Ben-Zion 2008; Brietzke *et al.* 2009; Dalguer & Day 2009). This general expectation is supported by our detailed observational results.

A number of studies tested the hypothesis that ruptures on bimaterial faults have a statistically preferred propagation direction, using asymmetry of rock damage across several large faults (Dor *et al.* 2006a,b, 2008; Lewis *et al.* 2005, 2007; Wechsler *et al.* 2009) and asymmetry of early aftershocks on the northern SAF (Rubin & Gillard 2000; Rubin 2002; Schorlemmer & Ben-Zion 2008). In this study we performed systematic analysis of symmetry properties of offspring seismic events in 25 fault zones in CA. The examined data are associated with fault zones having various degrees of velocity contrasts (Table 2), including prominent bimaterial faults (e.g. sections of the San Andreas and Hayward faults), cases of near zero average contrast (e.g. the eastern Garlock and the SAF south of Parkfield) and intermediate cases (e.g. the San Jacinto, Ellsinore and south Newport-Inglewood faults). The diversity of results expected for the different fault zones (Table 2), and our analyses of patterns on multiple space–time scales (Section 4), allow us to conduct strong statistical tests of the hypothesis that earthquakes on faults with significant velocity contrast have preferred propagation directions that may be predicted from the velocity contrast and sense of loading.

For faults with velocity contrast larger than about 5 per cent, we find clear statistical confirmations for two complementary effects that are consistent with the theoretical studies of bimaterial faults: (i) immediate spatially close offspring events tend to occur in the opposite along-strike direction, and (ii) later more-distant events tend to occur within the preferred propagation direction. On the other hand, in the no-to-mild contrast zones the offspring distribution is symmetric with respect to the parent at all examined time and spatial scales (see Figs 9 and 11). There exists clear correlation between the magnitude of the observed asymmetry and the degree of velocity contrast across faults: all examined zones with strong velocity contrasts exhibit strong asymmetry of seismicity, most sections with mild contrasts have mild asymmetries in the expected directions, and all cases with no velocity contrast have statistically symmetric patterns. The two possible exceptions are zones 3 and 46 (western Garlock and southern Calaveras faults, respectively), where there may be statistical signatures of asymmetric seismicity patterns in a sense that is opposite to those predicted from the available velocity images.

The methodology used in this study involves two steps: (i) cluster identification and (ii) asymmetry analysis within significant clusters. The cluster identification problem is solved using the bimodality of the space–time–energy NND between earthquakes (Figs 3b and 5a, c and e). Importantly, this bimodality is readily detected in a non-parametric way (Section 3.2), which eliminates a possibility for problem-driven data-fitting. The clusters examined in this study correspond, by and large, to classical aftershocks. This is confirmed by (i) a visual analysis of Landers aftershocks in Zaliapin *et al.* (2008); (ii) a visual analysis of clusters detected in this work (e.g. Fig. 6) and (iii) the fact that almost all clustered events lie within three rupture lengths from their parent, independently of the parent's magnitude (Figs 5a, c and e). The employed method of cluster identification is thus both (i) 'objective', as it does not involve any free choices (except the definition of the distance) and is completely driven by the statistical features of the data, and (ii) 'intuitive', since in most cases the results correspond to the commonly used definition of aftershocks.

The asymmetry analysis itself is quite straightforward, being focused on the average displacement of offspring earthquakes relative to their parent. The normalized distance R_{ij}—a core element of our complementary analyses of Sections 4.1 and 4.2—allows one to directly compare and average the results for different parent magnitudes and thus increases the significance of the findings. The asymmetry index A_k of eq. (5) is normalized to have the scale of a standard Normal random variable, which is useful for assessing the asymmetry significance. Specifically, the probability for a symmetric sequence to produce an asymmetry index larger than Q equals to the probability of a standard Normal random variable to be above Q. This, as well as the employed empirical percentile approach (see Fig. 9), virtually eliminates the possibility that the deviations from symmetry detected in the strong contrast zones are the result of random sample fluctuations. Furthermore, the average signed distance W from the parent, which is probably the most intuitive measure of asymmetry, indicates for strong contrast faults (Section 4.2, Fig. 11) not only small-scale asymmetry in the opposite direction, but also higher number of later and more distant events in the preferred direction. The units of W are the parent rupture lengths, which simplify the interpretation of the observed deviations from $W = 0$. The deviations in strong contrast zones shown in Fig. 11 are not only significant; their amplitude systematically increases for immediate offspring events and at small times they reach values that indicate a purely asymmetric (one-sided) offspring distribution. This provides further evidence that our results are not caused by random spatial fluctuations of the offspring events.

Rubin & Ampuero (2007) observed in simulations of ruptures on a bimaterial fault governed by slip-weakening friction that, under some conditions, when the main rupture is arrested a small daughter pulse can be generated near the tip at the preferred direction and propagate some distance further. They suggested that this may explain the enhanced early aftershocks over short distance in the opposite direction. Such daughter pulses provide a reasonable mechanism for asymmetric seismicity over short space–time scales, although they are relatively weak dynamical features that may be suppressed relatively easily by complexities expected to exist on natural faults (e.g. stress heterogeneities and off-fault yielding). Moreover, the small-scale daughter pulses do not explain the enhanced seismicity in the preferred direction over larger space–time scales seen in Fig. 11 for strong contrast faults. In the simulations of Rubin & Ampuero (2007) that produce macroscopically symmetric ruptures, the daughter pulses require special conditions for generation (e.g. large velocity contrast combined with a small drop of the friction coefficient and abrupt arrest of the main rupture). We also note that these simulations and related works with slip-weakening friction ignore the dependency of friction on the slip velocity, which is shown in laboratory experiments (e.g. Tsutsumi & Shimamoto 1997; Di Toro *et al.* 2004; Mizoguchi *et al.* 2006) to be significant for high slip-rates expected to exist (e.g. Ben-Zion 2001) during propagation of earthquake ruptures. Ampuero & Ben-Zion (2008) demonstrated that when a velocity-dependence of friction is included in the simulations, there is a statistical tendency of bimaterial ruptures to evolve under broad range of conditions (including stress heterogeneities and effects of off-fault yielding) towards unidirectional pulses in the preferred direction. Brietzke *et al.* (2009) showed with 3-D simulations that when ruptures on bimaterial strike-slip faults are large enough, so that the along-strike (mode II) propagation is dominant over the propagation in the depth direction (mode III), they tend to evolve for broad ranges of conditions (including stress heterogeneities) into predominantly unidirectional pulses in the preferred direction, even in the absence of velocity-dependent friction (see also Dalguer *et al.* 2009). These macroscopic rupture asymmetries produce stronger and larger scale effects than the daughter pulses, and they can explain both the small-scale enhancement of immediate aftershocks in the opposite direction (via asymmetric near-crack-tip mechanism of the type suggested by Rubin and

Ampuero) and the higher number of aftershocks in the preferred direction over larger scale-time scales (consistent with observations from large earthquakes).

In conclusion, the small-scale enhancement in the opposite direction provides evidence that bimaterial effects are important in natural tectonic settings, but not necessarily evidence for main shock directivity. The enhancement of aftershocks at larger distances in the preferred direction is consistent with preferential propagation of main shocks in the expected direction and the empirical association from large earthquakes between main shock directivity and aftershock productivity. Unequivocal tests of the preferred propagation direction hypothesis will require detailed analysis of rupture directivities of small events (e.g. McGuire 2004) along with high-resolution information on the velocity contrasts and earthquake locations (e.g. Thurber *et al.* 2006; Zhao *et al.* 2010). Our analysis has been motivated by the assumption that a statistical bias in the rupture behaviour of small earthquakes is relevant for the expected behaviour of large events on the same faults. This is likely to hold in this problem, since the dynamic effects associated with a velocity contrast increase with propagation distance along the bimaterial interface and are thus expected to be larger for larger events (e.g. Adams 1995; Ben-Zion and Huang 2002; Dalguer and Day 2009). Future studies should attempt to clarify the behaviour in zones 3 and 46 with higher resolution imaging of the local velocity contrasts and earthquake locations. Given the observed asymmetries of seismicity along zones 5 (Mojave Section of the SAF), 9 (South Newport-Inglewood), 11 (San Jacinto) and 12 (Ellsinore), and the close proximities of these zones to large urban areas in southern CA, it would also be useful to obtain additional higher-resolution information on the local velocity structures and seismicity in these zones.

ACKNOWLEDGMENTS

We thank Peter Powers for providing us the seismic catalogues analysed in this study. The manuscript benefited from useful comments by Allan Rubin, Peter Shearer and Editor Massimo Cocco. The research was supported by the Southern California Earthquake Center, the United States Geological Survey Grant G09AP00019 and the National Science Foundation Grants EAR-0844103, ATM-0620838 and EAR-0934871.

REFERENCES

Adams, G.G., 1995. Self-excited oscillations of two elastic half-spaces sliding with constant coefficient of friction, *J. appl. Mech.,* **62,** 867–872.

Ampuero, J.P. & Ben-Zion, Y., 2008. Cracks, pulses and macroscopic asymmetry of dynamic rupture on a bimaterial interface with velocity-weakening friction, *Geophys. J. Int.,* **173,** 674–692, doi: 10.1111/j.1365-246X.2008.03736.x.

Andrews, D.J. & Ben-Zion, Y., 1997. Wrinkle-like slip pulse on a fault between different materials, *J. geophys. Res.,* **102,** 553–571.

Atkinson, G.M. & Boore, D.M., 1997. Some comparisons between recent ground motion relations, *Seismol. Res. Lett.,* **68**(1), 24–40.

Baiesi, M & Paczuski, M., 2004. Scale-free networks of earthquakes and aftershocks. *Phys. Rev. E,* **69,** 066106, doi:10.1103/PhysRevE.69.066106.

Ben-Zion, Y., 1989. The response of two joined quarter spaces to SH line sources located at the material discontinuity interface, *Geophys. J. Int.,* **98,** 213–222.

Ben-Zion, Y., 1990. The response of two half spaces to point dislocations at the material interface, *Geophys. J. Int.,* **101,** 507–528.

Ben-Zion, Y., 2001. Dynamic rupture in recent models of earthquake faults, *J. Mech. Phys. Solids,* **49,** 2209–2244.

Ben-Zion, Y., 2008. Collective behavior of earthquakes and faults: continuum-discrete transitions, evolutionary changes and corresponding dynamic regimes, *Rev. Geophys.,* **46,** RG4006, doi:10.1029/2008RG000260.

Ben-Zion, Y. & Andrews, D. J., 1998. Properties and implications of dynamic rupture along a material interface, *Bull. seism. Soc. Am.,* **88,** 1085–1094.

Ben-Zion, Y. & Huang, Y., 2002. Dynamic rupture on an interface between a compliant fault zone layer and a stiffer surrounding solid, *J. geophys. Res.,* **107**(B2), 2042, doi:10.1029/2001JB000254.

Ben-Zion, Y. & Shi, Z., 2005. Dynamic rupture on a material interface with spontaneous generation of plastic strain in the bulk. *Earth. planet. Sci. Lett.,* **236,** 486–496, doi:10.1016/j.epsl.2005.03.025.

Ben-Zion, Y., Katz, S. & Leary, P., 1992. Joint inversion of fault zone head waves and direct *P* arrivals for crustal structure near major faults, *J. geophys. Res,* **97,** 1943-1951.

Brietzke, G.B., & Ben-Zion, Y., 2006. Examining tendencies of in-plane rupture to migrate to material interfaces, *Geophys. J. Int.,* **167,** 807–819, doi:10.1111/j.1365-246X.2006.03137.x.

Brietzke, G.B., Cochard, A. & Igel, H., 2009. Importance of bimaterial interfaces for earthquake dynamics and strong ground motion, *Geophys. J. Int.,* **178,** 921–938.

Dalguer, L.A. & Day, S.M., 2009. Asymmetric rupture of large aspect-ratio faults at bimaterial interface in 3D, *Geophys. Res. Lett.,* **36,** L23307, doi:10.1029/2009GL040303.

Davis, S.D. & Frohlich, C., 1991. Single-link cluster analysis, synthetic earthquake catalogs, and aftershock identification, *Geophys. J. Intl.,* **104**(2), 289–306.

Di Toro, G., Goldsby, D.L. & Tullis, T.E., 2004. Friction falls towards zero in quartz rock as slip velocity approaches seismic rates, *Nature,* **427,** 436–439.

Dor, O., Rockwell, T.K. & Ben-Zion, Y., 2006a. Geologic observations of damage asymmetry in the structure of the San Jacinto, San Andreas and Punchbowl faults in southern California: a possible indicator for preferred rupture propagation direction, *Pure appl. Geophys.,* **163,** 301–349.

Dor, O., Ben-Zion, Y., Rockwell, T.K. & Brune, J., 2006b. Pulverized rocks in the Mojave section of the San Andreas Fault Zone, *Earth planet. Sci. Lett.,* **245,** 642–654.

Dor, O., Yildirim, C., Rockwell, T.K., Ben-Zion, Y., Emre, O., Sisk, M. & Duman, T.Y., 2008. Geologic and geomorphologic asymmetry across the rupture zones of the 1943 and 1944 earthquakes on the North Anatolian Fault: possible signals for preferred earthquake propagation direction, *Geophys. J. Int.,* **173,** 483–504, doi:10.1111/j.1365-246X.2008.03709.x.

Dunham, E.M. & Rice, J.R., 2008. Earthquake slip between dissimilar poroelastic materials, *J. geophys. Res.,* **113,** B09304, doi:10.1029/2007JB005405.

Eberhart-Phillips, D. & Michael, A.J., 1993. Three-dimensional velocity structure, seismicity, and fault structure in the Parkfield region, central California, *J. geophys. Res.,* **98,** 15 737–15 758.

Eberhart-Phillips, D. & Michael, A.J., 1998. Seismotectonics of the Loma Prieta, California, region determined from three-dimensional V_p, V_p/V_s, and seismicity, *J. geophys. Res.,* **103,** 21 099–21 120.

Ellsworth, W. L., *et al*., 2000. Seismicity of the San Andreas Fault system in central California: application of the double-difference location algorithm on a regional scale, *EOS, Trans. Am. geophys. Un.,* **81**(48), Fall Meet. Suppl., Abstract S21D-01.

Feller, W., 1991. *An Introduction to Probability Theory and Its Applications,* Vol. 2, 2nd edn, Wiley, New York, NY.

Fuis, G.S., Ryberg, T., Godfrey, N., Okaya, D.A. & Murphy, J.M., 2001. Crustal structure and tectonics from the Los Angeles basin to the Mojave Desert, southern CA. *Geology,* **29,** 15–18.

Fuis, G.S. *et al*., 2003. Fault systems of the 1971 San Fernando and 1994 Northridge earthquakes, southern California: relocated aftershocks and seismic images from LARSE II, *Geology,* **31,** 171–174.

Gardner, J. K. & Knopoff, L., 1974. Is sequence of earthquakes in southern California, with aftershocks removed, Poissonian? *Bull. seism. Soc. Am.,* **64**(15), 1363–1367.

Gomberg, J., Reasenberg, P.A., Bodin, P. & Harris, R.A., 2001. Earthquake triggering by seismic waves following the Landers & Hector Mine earthquakes, *Nature,* **411,** 462–465.

Harris, R. & Day, S.M., 1997, Effect of a low-velocity zone on a dynamic rupture, *Bull. seism. Soc. Am.,* **87,** 1267–1280.

Hauksson, E., & Shearer, P.M., 2005. Southern California hypocenter relocation with waveform cross-correlation, Part 1: results using the double-difference method, *Bull. seism. Soc. Am.,* **95**(3), 896–903.

Hill, D.P. & Prejean, S.G., 2007. Dynamic triggering, in *Earthquake Seismology: Treatise on Geophysics,* Vol. 4, pp. 257–291, eds Kanamori, H. & G. Schubert, Elsevier, Amsterdam.

Hill, D.P. *et al*., 1993. Seismicity remotely triggered by the magnitude 7.3 Landers, California, earthquake, *Science,* **260,** 1617–1622.

Lewis, M.A, Peng, Z., Ben-Zion, Y. & Vernon, F., 2005. Shallow seismic trapping structure in the San Jacinto fault zone, *Geophys. J. Int.,* **162,** 867–881.

Lewis, M.A, Ben-Zion, Y. & McGuire, J., 2007. Imaging the deep structure of the San Andreas Fault south of Hollister with joint analysis of fault-zone head and direct P arrivals, *Geophys. J. Int.,* **169,** 1028–1042.

Marsan, D. & Lengline, O., 2008. Extending earthquakes' reach through cascading, *Science,* **319,** 1076–1079, doi:10.1126/science.1148783.

McGuire, J.J., 2004. Estimating finite source properties of small earthquake ruptures, *Bull. seism. Soc. Am.,* **94,** 377–393.

McGuire, J. & Ben-Zion, Y., 2005. High-resolution imaging of the Bear Valley section of the San Andreas Fault at seismogenic depths with fault-zone head waves and relocated seismicity, *Geophys. J. Int.,* **163,** 152–164, doi:10.1111/j.1365-246X.2005.02703.x.

Michael, A.J., & Eberhart-Phillips, D., 1991. Relations among fault behavior, subsurface geology, and three-dimensional velocity models, *Science,* **253,** 651–654.

Mizoguchi, K., Hirose, T., Shimamoto, T. & Fukuyama, E., 2006. Moisture related weakening and strengthening of a fault activated at seismic slip rates, *Geophys. Res. Lett.,* **33,** L16319, doi:10.1029/2006GL026980.

Molchan, G.M. & Dmitrieva, O.E., 1992. Aftershock identification: methods and new approaches, *Geophys. J. Int.,* **109**(3), 501–516.

Ohlendorf, S., Peng, Z., & Ben-Zion, Y., 2007. Velocity contrast along the Hayward fault from analysis of fault zone head waves, *EOS, Trans. Am. geophys. Un.,* **88**(52), Fall Meet. Suppl., Abstract S21A-0237.

Powers, P.M., 2009. Seismicity distribution near strike-slip faults in California, *PhD thesis*. University of Southern California.

Powers, P.M. & Jordan, T.H., 2010. Distribution of seismicity across strike-slip faults in California, *J. geophys. Res,* **115,** B05305, doi:10.1029/2008JB006234.

Ranjith, K. & Rice, J., 2001. Slip dynamics at an interface between dissimilar materials, *J. Mech. Phys. Solids,* **49,** 341–361.

Reasenberg, P, 1985. Second order moment of central California seismicity, 1969-1982, *J. geophys. Res.,* **90,** 5479–5495.

Rubin, A.M., 2002. Aftershocks of microearthquakes as probes of the mechanics of rupture, *J. geophys. Res.,* **107,** 2142, doi:10.1029/2001JB000496.

Rubin, A.M. & Ampuero, J.P., 2007. Aftershock asymmetry on a bimaterial interface, *J. geophys. Res.,* **112,** B05307, doi:10.1029/2006JB004337.

Rubin, A. & Gillard, D., 2000. Aftershock asymmetry/rupture directivity along central San Andreas fault microearthquakes, *J. geophys. Res.,* **105,** 19 095–19 109.

Rudnicki, J.W., & Rice, J.R., 2006. Effective normal stress alteration due to pore pressure changes induced by dynamic slip propagation on a plane between dissimilar materials, *J. geophys. Res.,* **111,** B10308, doi:10.1029/2006JB004396.

Schorlemmer, D. & Ben-Zion, Y., 2008, Directivity effects of fault velocity contrast on triggered seismicity, *Seism. Res. Lett.,* **79**(2), 295.

Scott, J.S., Masters, T.G. & Vernon, F.L., 1994. 3-D velocity structure of the San Jacinto fault zone near Anza, California—I. *P* waves. *Geophys. J. Int.,* **119,** 611–626.

Shearer, P.M., Hauksson, E. & Lin, G., 2005. Southern California hypocenter relocation with waveform cross-correlation, Part 2: results using source-specific station terms and cluster analysis, *Bull. seism. Soc. Am.,* **95**(3), 904–915.

Shi, Z. & Ben-Zion, Y., 2006. Dynamic rupture on a bimaterial interface governed by slip-weakening friction, *Geophys. J. Int.,* **165,** 469–484.

Stein, R.S., Barka, A.A. & Dieterich, J.H., 1997. Progressive failure on the North Anatolian fault since 1939 by earthquake stress triggering, *Geophys. J. Int.,* **128,** 594–604.

Sturtevant, B., Kanamori, H. & Brodsky, E.E., 1996. Seismic triggering by rectified diffusion in geothermal systems, *J. geophys. Res.,* **101,** 25 269–25 282, doi:10.1029/96JB02654.

Tape, C., Liu, Q., Maggi, A. & Tromp, J., 2009. Adjoint tomography of the southern California crust, *Science,* **325,** 988–992.

Thurber, C., Roecker, S., Ellsworth, W., Chen, Y., Lutter, W. & Sessions, R., 1997. Two-dimensional seismic image of the San Andreas Fault in the Northern Gabilan Range, central California: evidence for fluids in the fault zone, *Geophys. Res. Lett.,* **24,** 1591–1594.

Thurber, C.H., Zhang, H., Waldhauser, F., Hardebeck, J., Michael, A. & Eberhart-Phillips, D., 2006. Three-dimensional compressional wavespeed model, earthquake relocations, and focal mechanisms for the Parkfield, California, region, *Bull. seism. Soc. Am.,* **96**(4B), S38–S49, doi:10.1785/0120050825.

Thurber, C.H., Brocher, T.M., Zhang, H. & Langenheim, V.E., 2007. Three-dimensional *P* wave velocity model for the San Francisco Bay region, California, *J. geophys. Res.,* **112,** B07313, doi:10.1029/2006JB004682.

Tsutsumi, A. & Shimamoto, T., 1997. High-velocity frictional properties of Gabbro, *Geophys. Res. Lett.,* **24,** 699–702.

Venables W.N. & Ripley, B.D., 2002. *Modern Applied Statistics with S,* 4th edn, Springer, New York, NY.

Wechsler, N., Rockwell, T.K. & Ben-Zion, Y., 2009. Analysis of rock damage asymmetry from geomorphic signals along the trifurcation area of the San-Jacinto Fault, *Geomorphology,* **113,** 82–96, doi:10.1016/j.geomorph.2009.06.007.

Weertman, J., 1980. Unstable slippage across a fault that separates elastic media of different elastic constants, *J. geophys. Res.,* **85,** 1455–1461.

Zaliapin, I., Gabrielov, A., Wong, H. & Keilis-Borok, V., 2008. Clustering analysis of seismicity and aftershock identification, *Phys. Rev. Lett.,* **101,** doi:10.1103/PhysRevLett.101.018501.

Zhao, P. & Peng, Z., 2008. Velocity contrast along the Calaveras fault from analysis of fault zone head waves generated by repeating earthquakes, *Geophys. Res. Lett.,* **35,** L01303, doi:10.1029/2007GL031810.

Zhao, P., Peng, Z., Shi, Z., Lewis, M. & Ben-Zion, Y., 2010. Variations of the velocity contrast and rupture properties of *M*6 earthquakes along the Parkfield Section of the San Andreas Fault, *Geophys. J. Int.,* **180,** 765–780, doi:10.1111/j.1365-246X.2009.04436.x.

Zhuang, J., Ogata, Y. & Vere-Jones, D., 2002. Stochastic declustering of space-time earthquake occurrences, *J. Am. Stat. Assoc.,* **97**(458), 369–380.

Zhuang, J.C., Ogata, Y., Vere-Jones, D., 2004. Analyzing earthquake clustering features by using stochastic reconstruction, *J. geophys. Res.,* **109**(B5), B05301, doi:10.1029/2003JB002879.